

REPORT DOCUMENTATION PAGE

1a. REPORT SECURITY CLASSIFICATION Unclassified		1b. RESTRICTIVE MARKINGS										
2a. SECURITY CLASSIFICATION AUTHORITY		3. DISTRIBUTION/AVAILABILITY OF REPORT Approved for Public Release; distribution unlimited.										
2b. DECLASSIFICATION/DOWNGRADING SCHEDULE												
4. PERFORMING ORGANIZATION REPORT NUMBER(S) <u>UTRC Report-R87-957333-1</u>		5. MONITORING ORGANIZATION REPORT NUMBER(S)										
6a. NAME OF PERFORMING ORGANIZATION United Tech. Research Center	6b. OFFICE SYMBOL (If applicable)	7a. NAME OF MONITORING ORGANIZATION Turbopropulsion Laboratory, Code 67SF										
6c. ADDRESS (City, State, and ZIP Code) Silver Lane East Hartford, CT 06108		7b. ADDRESS (City, State, and ZIP Code) Naval Postgraduate School Monterey, CA 93943										
8a. NAME OF FUNDING/SPONSORING ORGANIZATION Naval Air Systems Command	8b. OFFICE SYMBOL (If applicable)	9. PROCUREMENT INSTRUMENT IDENTIFICATION NUMBER N00014-85-C-0702										
8c. ADDRESS (City, State, and ZIP Code) Department of the Navy Washington, D.C. 20361		10. SOURCE OF FUNDING NUMBERS PROGRAM ELEMENT NO. PROJECT NO. TASK NO. WORK UNIT ACCESSION NO.										
11. TITLE (Include Security Classification) The Unsteady Flow in the Far-Field of an Isolated Blade Row												
12. PERSONAL AUTHOR(S) Joseph M. Verdon												
13a. TYPE OF REPORT Final Report	13b. TIME COVERED FROM 9/85 TO 4/87	14. DATE OF REPORT (Year, Month, Day) April, 1987	15. PAGE COUNT 66									
16. SUPPLEMENTARY NOTATION Final Report. Project Manager: Dr. Raymond P. Shreeve, Turbopropulsion Laboratory, Code 67SF Naval Postgraduate School, Monterey, CA 93943												
17. COSATI CODES <table border="1"><tr><th>FIELD</th><th>GROUP</th><th>SUB-GROUP</th></tr><tr><td></td><td></td><td></td></tr><tr><td></td><td></td><td></td></tr></table>		FIELD	GROUP	SUB-GROUP							18. SUBJECT TERMS (Continue on reverse if necessary and identify by block number) Unsteady Velocity Potential; Isolated, Two-Dimensional Blade-Row; Far Field Acoustic Response; Vortical Response; Subsonic Transonic, Supersonic Inlet/Exit Conditions	
FIELD	GROUP	SUB-GROUP										
19. ABSTRACT (Continue on reverse if necessary and identify by block number) This report describes a theoretical investigation of the unsteady flow in the far field of an isolated two-dimensional blade row. In particular, analytic far-field solutions are derived for cascades operating at subsonic, transonic and supersonic inlet and exit Mach numbers. These solutions describe the velocity potential fluctuations associated with irrotational pressure (acoustic) disturbances, rotational velocity disturbances and the vorticity shed from blade trailing edges and convected along blade wakes. As such they provide the inlet and exit information needed for a successful numerical resolution of the unsteady flow through the cascade. As part of this investigation a convenient method for classifying unsteady excitations, based on the acoustic response in the far field, is provided. Also, analytical results are presented to illustrate subsonic and supersonic far-field acoustic response behavior and numerical solutions have been determined for subsonic compressor cascades to demonstrate partially the impact of unsteady far-field behavior on the aerodynamic response at a vibrating blade surface.												
20. DISTRIBUTION/AVAILABILITY OF ABSTRACT <input checked="" type="checkbox"/> UNCLASSIFIED/UNLIMITED <input type="checkbox"/> SAME AS RPT. <input type="checkbox"/> DTIC USERS		21. ABSTRACT SECURITY CLASSIFICATION										
22a. NAME OF RESPONSIBLE INDIVIDUAL		22b. TELEPHONE (Include Area Code)	22c. OFFICE SYMBOL									

UFRG R87-957333-1 }

LIBRARY
RESEARCH REPORTS DIVISION
NAVAL POSTGRADUATE SCHOOL
MONTEREY, CALIFORNIA 93940



Report R87-957333-1

THE UNSTEADY FLOW IN THE FAR FIELD OF AN ISOLATED BLADE ROW.

by

Joseph M. Verdon

Final Report

Prepared Under Contract N00014-85-C-0702

for the

^{ae} Naval Air Systems Command,
Department of the Navy
Washington, D.C. 20361

April 1987

The Unsteady Flow in the Far Field of an Isolated Blade Row

SUMMARY

This report describes a theoretical investigation of the unsteady flow in the far field of an isolated two-dimensional blade row. In particular, analytic far-field solutions are derived for cascades operating at subsonic, transonic and supersonic inlet and exit Mach numbers. These solutions describe the velocity potential fluctuations associated with irrotational pressure (acoustic) disturbances, rotational velocity disturbances and the vorticity shed from blade trailing edges and convected along blade wakes. They thus provide the inlet and exit boundary-condition information needed for a proper numerical resolution of the unsteady flow through the cascade. As part of this investigation a convenient method for classifying unsteady excitations based on the acoustic response in the far field is developed and analytical results are presented to illustrate subsonic and supersonic far-field acoustic response behavior. Numerical calculations have also been carried out for unsteady flows through subsonic compressor-type cascades to demonstrate the results of matching analytic far-field to numerical near-field solutions and, to some extent, the impact of unsteady far-field behavior on the aerodynamic response at a vibrating blade surface.

The Unsteady Flow in the Far Field of an Isolated Blade Row**TABLE OF CONTENTS**

1. INTRODUCTION.....	1
2. PHYSICAL PROBLEM AND GOVERNING EQUATIONS.....	3
2.1 Governing Equations in the Far Field.....	5
3. UNSTEADY FAR-FIELD SOLUTIONS.....	7
3.1 Preliminaries.....	7
3.2 The Potential due to Acoustic Response Disturbances.....	8
4. THE UNSTEADY POTENTIAL DUE TO VORTICAL DISTURBANCES...	13
4.1 The Rotational Velocity in the Far Downstream Region.....	13
4.2 The Potential due to Vortical Disturbances.....	15
4.3 The Complete Solution for the Unsteady Potential.....	16
4.4 Implementation of Far-Field Solutions in Numerical Computations.....	17
5. UNSTEADY FLOW BEHAVIOR IN THE FAR FIELD.....	19
5.1 Classification of Unsteady Excitations.....	19
5.2 The Acoustic Response in The Far Field.....	20
5.3 The Potential Response to Vortical Disturbances.....	24
6. NUMERICAL EXAMPLES: SUBSONIC FLOW.....	25
6.1 Flat-Plate Cascade.....	26
6.2 DCA Cascade.....	28
7. CONCLUDING REMARKS.....	32
REFERENCES.....	33
LIST OF FIGURES.....	35
FIGURES 1 THROUGH 19.....	37

1. INTRODUCTION

There is an ongoing need to develop more complete unsteady aerodynamic prediction methods for aeroelastic and aeroacoustic applications. Currently, linearized unsteady aerodynamic analyses in which unsteady fluctuations are regarded as small-amplitude perturbations of a nonuniform isentropic and irrotational mean or steady flow are receiving considerable attention (for recent reviews see Atassi 1987 and Verdon 1987a,b), particularly for turbomachinery aeroelastic applications (Atassi & Akai 1980; Caruthers 1981; Whitehead 1982; Verdon & Caspar 1982, 1984). In this situation the unsteady flow is excited by prescribed small-amplitude temporally and spatially periodic structural and external aerodynamic disturbances, and the complex amplitudes of the dependent linearized unsteady flow variables are governed by a system of linear time-independent equations which contain variable coefficients that depend on the underlying mean flow.

As a consequence of this linearization, boundary conditions at moving solid surfaces and jump conditions at moving wakes and shocks can be imposed at the mean positions of such surfaces. Also, for turbomachinery applications the required solution domain can be limited to a single extended blade-passage region. Moreover, analytical far-field solutions can be determined and matched to numerical near-field solutions; hence, this solution domain can be restricted further to a single blade passage region of finite extent in the axial direction. These features lead to economical and therefore technologically useful unsteady aerodynamic response predictions.

In this report analytic solutions for the unsteady velocity potential response far upstream and far downstream of an isolated two-dimensional blade row are determined. We consider the general unsteady cascade problem in which the unsteady flow is produced by structural (i.e., blade motions) and/or external aerodynamic excitations (i.e., incident acoustic, entropic or vortical gusts) and provide solutions for compressor- and turbine-type cascades operating under subsonic, transonic and supersonic inlet and exit conditions. Fourier series solutions will be determined for the continuous velocity potential fluctuations associated with the acoustic response in the far upstream and far downstream regions as well as for the continuous potential fluctuations in the far downstream region associated with the rotational velocity disturbances that are convected through the blade row. A closed form solution will be determined for the discontinuous potential fluctuation associated with the concentrated vorticity convected along blade wakes. The specific form of the solution for the potential due to acoustic response fluctuations depends upon whether the free-stream Mach number, M , is less than or greater than one, the free-stream flow angle, Ω , is positive or negative, the axial Mach number, $M \cos \Omega$, is less than or greater than one and the temporal frequency, ω , of the unsteady motion is positive or negative. A single solution holds for the potential fluctu-

ation associated with rotational velocity fluctuations and concentrated wake vorticity regardless of the sign of $M - 1$, Ω , $M \cos \Omega - 1$ or ω .

The complete solution for the velocity potential in the far field provides the inlet and exit information needed for the linearized unsteady aerodynamic analyses intended for blade aeroelastic and aeroacoustic design predictions. Moreover, a knowledge of the unsteady aerodynamic response in the far field is a prerequisite to guide the choice of computational grid spacings needed to resolve accurately the unsteady flow through the blade row, particularly for cascades operating at high subsonic or supersonic inlet and exit Mach numbers or subjected to high-frequency unsteady excitations. Such information should also be useful for constructing time-accurate numerical simulations (e.g., see Rai 1985; Fransson & Pandolfi 1986; Giles 1987) of nonlinear unsteady flows through turbomachine cascades.

Once the complete far-field solution is given below, the far-field acoustic response is studied leading to a useful classification of unsteady excitations. In addition, the results of parametric studies are presented to illustrate the acoustic response behavior in the far field at various free-stream Mach numbers and flow angles. Finally, we present numerical solutions for unsteady flows through subsonic compressor-type cascades to demonstrate the results that can be achieved by matching analytic far-field solutions to numerical near-field solutions and to illustrate the effects of the far-field acoustic response on the aerodynamic response (i.e., surface pressures and unsteady airloads) at a vibrating blade surface.

2. PHYSICAL PROBLEM AND GOVERNING EQUATIONS

We consider the time-dependent two-dimensional adiabatic flow, with negligible body forces, of an inviscid non-heat-conducting perfect gas through a cascade of airfoils or blades such as the one shown in figure 1. All physical quantities are dimensionless. Lengths have been scaled with respect to blade chord, time with respect to the ratio of blade chord to the upstream free-stream speed, density and velocity with respect to the upstream free-stream density and velocity, respectively, and pressure with respect to the product of the upstream free-stream density and the square of the upstream free-stream speed. The mean or steady state positions of the blade chord lines coincide with the line segments $\eta = \xi \tan \Theta + mG$, $0 \leq \xi \leq \cos \Theta$, where ξ and η are Cartesian axes attached to the blade row and pointing in the axial-flow and the cascade “circumferential” directions, respectively, $m = 0, 1, 2, \dots$ is a blade number index, Θ is the cascade stagger angle and \vec{G} is the cascade gap vector which is directed along the η -axis with magnitude equal to the blade spacing.

In the absence of unsteady excitation the flow beyond some finite distance upstream (say $\xi < \xi_-$) and downstream ($\xi > \xi_+$) from the blade row is assumed to be at the most a small irrotational steady perturbation from a uniform free stream. In addition, the unsteady flow remains attached to the blade surfaces and therefore, thin vortex sheets or unsteady wakes emanate from the blade trailing edges and extend downstream. Finally, any shocks that might occur are assumed to be of weak to moderate strength and have small curvature. Thus, changes in the entropy and vorticity of a fluid particle as it passes through a shock are regarded as negligible.

The time-dependent or unsteady fluctuations in the flow arise from one or more of the following sources: blade motions, upstream and/or downstream acoustic disturbances which carry energy toward the blade row, and upstream entropic and vortical disturbances which are convected through the blade row. These excitations are assumed to be of small amplitude and periodic in time. The external aerodynamic excitations are also spatially periodic, while the blade motion is periodic in the cascade- or η -direction. For example, we consider blade motions of the form

$$\vec{\mathcal{R}}(\vec{X} + m\vec{G}, t) = \text{Re}\{\vec{r}(\vec{X}) \exp[i(\omega t + m\sigma)]\}, \quad \vec{X} \text{ on } B. \quad (2.1)$$

In (2.1) $\vec{\mathcal{R}}$ measures the displacement of a point on a moving blade surface relative to its mean or steady-state position, \vec{X} is a position vector, t is time, \vec{r} is a complex displacement-amplitude vector, ω is the frequency of the blade motion, σ is the phase angle between the motions of adjacent blades, $\text{Re}\{\}$ denotes the real part of $\{\}$ and B denotes the reference ($m = 0$) blade surface. Incident disturbances are of the form

$$\tilde{p}_I(\vec{X}, t) = \text{Re}\{p_{I,\mp\infty} \exp[i(\vec{\kappa}_{\mp\infty} \cdot \vec{X} + \omega t)]\}, \quad \xi \leq \xi_{\mp}, \quad (2.2)$$

where $p_{I,\mp\infty}$ and $\vec{\kappa}_{\mp\infty}$ are the amplitude and wave number, respectively, of an incident pressure fluctuation, $\tilde{p}_I(\vec{X}, t)$, coming from far upstream ($-\infty$) or far downstream (∞) and carrying energy towards the blade row.

Note that the interblade phase angle, σ , of an incident disturbance is $\vec{\kappa}_{\mp\infty} \cdot \vec{G}$. Also, the temporal frequency and wave number of an incident entropic or vortical disturbance are related by $\omega = -\vec{\kappa}_{-\infty} \cdot \vec{V}_{-\infty}$ where $\vec{V}_{-\infty}$ is the uniform relative inlet velocity, but a more complicated relationship exists between ω and $\vec{\kappa}_{\mp\infty}$ for an incident pressure disturbance as will become clear from the discussion below.

For small-amplitude unsteady excitations, i.e., $|\vec{r}|, |p_{I,\mp\infty}|$, etc. $\sim \mathcal{O}(\epsilon) \ll 1$, the time-dependent flow can be regarded as a small perturbation about an underlying mean flow. In addition, because of our assumptions regarding shocks and the flow far upstream of the blade row, the underlying mean or steady flow, which is assumed to be known in the present study, will be isentropic and irrotational. Thus $\vec{V} = \nabla\Phi$ and

$$(M_{-\infty} V/M)^2 = (M_{-\infty} A)^2 = \bar{\rho}^{(\gamma-1)} = (\gamma M_{-\infty}^2 P)^{(\gamma-1)/\gamma} \\ = 1 - \frac{(\gamma-1)}{2} M_{-\infty}^2 [(\nabla\Phi)^2 - 1] = \frac{2 + (\gamma-1)M_{-\infty}^2}{2 + (\gamma-1)M^2} , \quad (2.3)$$

where $\vec{V}, \Phi, \bar{\rho}, M, P$ and A are the local steady-flow velocity, velocity potential, density, Mach number, pressure and speed of sound propagation, respectively, and γ is the specific heat ratio of the fluid. Finally, because of the assumed form of the unsteady excitations, the first-order flow properties must be harmonic in time, e.g., $\tilde{p}(\vec{X}, t) = Re\{p(\vec{X})e^{i\omega t}\}$, and they must satisfy the blade-to-blade periodicity condition, i.e.,

$$p(\vec{X} + m \vec{G}) = p(\vec{X})e^{im\sigma} . \quad (2.4)$$

Thus the complex amplitudes of the linearized unsteady flow variables can be determined by solving a time-independent set of governing equations, and numerical solutions to these equations are required only over a single extended blade-passage region.

The field equations governing the first-order unsteady flow can be written as (Goldstein 1978, 1979)

$$\frac{\bar{D}s}{Dt} = 0 , \quad (2.5)$$

$$\frac{\bar{D}}{Dt} (\vec{v}^R - s \nabla\Phi/2) + [(\vec{v}^R - s \nabla\Phi/2) \cdot \nabla] \nabla\Phi = 0 , \quad (2.6)$$

and

$$\frac{\bar{D}}{Dt} (A^{-2} \frac{\bar{D}\phi}{Dt}) - \bar{\rho}^{-1} \nabla \cdot (\bar{\rho} \nabla\phi) = \bar{\rho}^{-1} \nabla \cdot (\bar{\rho} \vec{v}^R) . \quad (2.7)$$

Here s , \vec{v}^R and ϕ are the complex amplitudes of the first-order entropy, rotational velocity and velocity potential, respectively, and $\bar{D}/Dt = i\omega + \vec{V} \cdot \nabla$ is a mean flow convective derivative operator. The complex amplitude of the first-order velocity is given by $\vec{v} = \nabla\phi + \vec{v}^R$. The rotational velocity is divergence free far upstream of the blade row, and the unsteady pressure fluctuation is related directly to the velocity

potential by $p = -\bar{\rho} \bar{D}\phi/Dt$. In general we require a solution to the foregoing system of equations which is subject to the condition of flow tangency at blade surfaces (attached flow), appropriate jump conditions across shocks and blade wakes, and the requirement that acoustic response disturbances either attenuate or propagate away from or parallel to the blade row in the far field (Verdon 1987a,b). As a consequence of the small unsteady disturbance approximation, surface conditions can be imposed at the mean positions of the blade, shock and “wake”, i.e., the downstream stagnation streamlines, surfaces with mean shock and wake locations being determined from the nonlinear steady solution.

The system of linearized unsteady equations can be solved sequentially to determine the fluctuations in entropy, rotational velocity and velocity potential throughout an extended blade passage solution domain. The entropic and rotational velocity fluctuations are convected by the mean flow and therefore can be determined in terms of prescribed upstream (i.e., on $\xi = \xi_-$) entropic and rotational velocity distributions. Information on the velocity potential fluctuation is required in both the far upstream and far downstream regions of the flow. Moreover, this information cannot be provided *a priori* as it depends on the response of the blading to an imposed unsteady excitation. However, analytic solutions for the potential in the far field can be determined. These can be matched to a (numerical) near-field solution and thereby serve to complete the specification of the linearized unsteady boundary-value problem. This feature also permits the numerical solution domain to be limited to a single extended blade passage region of finite extent (i.e., $\xi_- < \xi < \xi_+$) in the axial-flow direction.

2.1 Governing Equations in the Far Field

In the far upstream and far downstream regions the steady background flow is at most a small perturbation (of $\mathcal{O}(\epsilon)$) from a uniform free stream. Therefore it follows from (2.7) that far from the blade row and to within first-order in ϵ , the unsteady potential is governed by the constant-coefficient differential equation of classical linearized unsteady aerodynamic theory (see Miles 1959; Ashley & Landahl 1961); i.e.,

$$(\nabla^2 - A_{\mp\infty}^{-2} \frac{\bar{D}_{\mp\infty}^2}{Dt^2})\phi = -\nabla \cdot \vec{v}^R, \quad \xi \gtrless \xi_{\mp}. \quad (2.8)$$

It also follows from (2.6) that the rotational velocity is governed by

$$\frac{\bar{D}_{\mp\infty}}{Dt} \vec{v}^R = (iw + \vec{V}_{\mp\infty} \cdot \nabla) \vec{v}^R = 0. \quad (2.9)$$

Note that under our present assumptions $\nabla \cdot \vec{v}^R = 0$ in the far upstream region and therefore the far upstream velocity potential fluctuations are caused by acoustic disturbances only.

We will require analytic solutions to (2.8) for periodic (in η) but otherwise arbitrary potential distributions at the axial locations $\xi = \xi_{\mp}$ and, as a consequence, to

(2.9) for periodic but otherwise arbitrary rotational velocity distributions on $\xi = \xi_+$. These solutions must satisfy the blade-to-blade periodicity condition (2.4) and also the conditions of continuity of pressure and normal velocity across blade wakes; i.e.,

$$\frac{\bar{D}_\infty}{Dt} [\phi] = 0 \quad \text{or} \quad [\phi] = [\phi]_{Ref} \exp[i m(\sigma - T_m/V_\infty)], \quad \vec{X} \text{ on } W_m, \quad \xi > \xi_+, \quad (2.10)$$

and

$$[\nabla \phi] \cdot \vec{n} = -[\vec{v}^R] \cdot \vec{n}, \quad \vec{X} \text{ on } W_m, \quad \xi > \xi_+, \quad (2.11)$$

respectively. In addition, the potential ϕ must obey the condition that acoustic response waves either attenuate or propagate away from or parallel to the blade row in the far field. In (2.10) and (2.11) the symbol $[\]$ refers to the difference (upper – lower) in a flow quantity across a wake, $[\]_{Ref}$ is the value of $[\]$ at the point of intersection (ξ_+, η_+) of the reference ($m = 0$) wake and the axial line $\xi = \xi_+$ and T_m is a coordinate measuring distance in the direction of \vec{V}_∞ downstream from the line $\xi = \xi_+$. Note that to within first-order in ϵ , the mean wake positions, W_m , far downstream of the blade row can be regarded as an array of straight lines parallel to the free-stream flow direction. We require such solutions for subsonic ($M_{\mp\infty} < 1$) and supersonic ($M_{\mp\infty} > 1$) relative inlet and exit conditions. However in the supersonic case, we are interested primarily in flows having subsonic axial velocity component, i.e., $M_{\mp\infty} \cos \Omega_{\mp\infty} < 1$ since this is the situation of practical interest for axial-flow turbomachines.

3. UNSTEADY FAR-FIELD SOLUTIONS

3.1 Preliminaries

To determine solutions for the unsteady potential in the far field it is convenient to set

$$\phi(\vec{X}) = \phi^P(\vec{X}) + \phi^R(\vec{X})U(\xi - \xi_+) \quad \text{for } \xi \leq \xi_\mp , \quad (3.1)$$

where $\phi^P(\vec{X})$ is a continuous function which accounts for the fluctuations in the velocity potential due to irrotational pressure or acoustic disturbances, $\phi^R(\vec{X})$ accounts for the fluctuations in the potential in the far downstream region due to rotational velocity disturbances (including those due to the vorticity shed at blade trailing edges and convected along the blade wakes) and $U(x)$ is the unit step function. The latter disturbances are convected as vorticity waves by the underlying uniform flow and have no associated pressure or density fluctuations (Smith 1971). Therefore,

$$\frac{\bar{D}_\infty}{Dt} \phi^R = 0 \quad (3.2)$$

and it follows from (2.8) that

$$\nabla^2 \phi^R = -\nabla \cdot \vec{v}^R . \quad (3.3)$$

The potential component ϕ^P is a homogeneous solution of (2.8) which is continuous in \vec{X} and satisfies the cascade periodicity and acoustic wave propagation requirements stated above. The component ϕ^R is a particular solution of (2.8) (or (3.2) and (3.3)) which satisfies the cascade periodicity requirement and the wake jump conditions (2.10) and (2.11). We seek first a solution for the component of the velocity potential describing the acoustic response in the far upstream and far downstream flow regions in Section (3.2) and then proceed to determine a solution for the component of the potential describing the response to vortical waves in Section (4.2). The potential component ϕ^R depends on the rotational velocity fluctuations in the far downstream region, and a solution describing these fluctuations will be given in Section (4.1). We will use the independent variables, (ξ, η) and (T_m, N_m) , for determining the required solutions. The T_m, N_m -Cartesian axes are parallel and normal, respectively, to the mth wake in the far downstream region and have their origins at the intersection of mth wake and the line $\xi = \xi_+$ (see figure 1). Therefore we can write

$$T_m + iN_m = [\xi - \xi_+ + i(\eta - \eta_+ - mG)] \exp(-i\Omega_\infty) . \quad (3.4)$$

Unit vectors in a given coordinate direction, say the ξ -direction, are indicated by \vec{e}_ξ .

3.2 The Potential due to Acoustic Response Disturbances

To simplify the discussion in this section we will determine $\phi^P(\vec{X})$ for acoustic response disturbances only. Once this solution is obtained, it becomes a simple matter to add to it the appropriate terms that account for incident acoustic excitations. Also, we will omit the subscripts $\mp\infty$ when referring to free-stream flow properties, but it must be recalled that the symbols V , Ω , M , etc. represent either inlet or exit free-stream flow properties. Finally, the following derivation applies to subsonic ($M < 1$), transonic (in the limit $M \rightarrow 1$) and supersonic ($M > 1$) flows. However, it is restricted to flows with subsonic axial velocity component, i.e., $M \cos \Omega < 1$. Thus if $M > 1$, $|\tan \Omega| > (M^2 - 1)^{1/2}$, where Ω is the free-stream flow angle and $\pm \tan^{-1}[(M^2 - 1)^{1/2}]$ are the angles between the flow Mach waves (or characteristic lines) and the free-stream flow direction. Once this derivation is completed, we will simply present for the sake of completeness the appropriate results for supersonic axial flows ($M \cos \Omega > 1$).

The desired solution for the unsteady potential component ϕ^P can be determined by Fourier methods. Thus we consider periodic fundamental solutions of the form

$$\phi_n^P(\xi, \eta) = f_n(\xi) \exp(ik_{\eta,n}\eta), \quad n = 0, \pm 1, \pm 2, \dots, \quad (3.5)$$

where we use the symbol \vec{k} to denote the wave number of a response fluctuation and $k_{\eta,n} = (\sigma + 2\pi n)G^{-1}$ is a wave number in the cascade circumferential or η -direction. After substituting (3.5) into the far-field differential equation (2.8) and solving the resulting ordinary differential equation for f_n , we find that

$$f_n(\xi) = \begin{cases} a_{1,n} \exp(\chi_{1,n}\xi) + a_{2,n} \exp(\chi_{2,n}\xi) & \text{for } d_n^2 \neq 0 \\ (a_{1,n} + a_{2,n}\xi) \exp(\chi_{1,n}\xi) & \text{for } d_n^2 = 0 \end{cases}, \quad (3.6)$$

where

$$\begin{aligned} \chi_{\frac{1}{2},n} &= \pm d_n + iM^2 \delta_n \cos \Omega, \\ \delta_n &= (\omega V^{-1} + k_{\eta,n} \sin \Omega) / (1 - M^2 \cos^2 \Omega), \\ d_n^2 &= (1 - M^2 \cos^2 \Omega)^{-1} k_{\eta,n}^2 - M^2 \delta_n^2 \end{aligned} \quad (3.7)$$

and d_n is the principal root of d_n^2 ; i.e.,

$$d_n = \begin{cases} |d_n|, & \text{if } d_n^2 > 0 \\ i|d_n|, & \text{if } d_n^2 < 0 \end{cases}. \quad (3.8)$$

If $d_n^2 \neq 0$, each fundamental solution describes two wave-like disturbances which, depending upon the sign of d_n^2 , either grow or decay exponentially in the axial direction ($d_n^2 > 0$) or propagate carrying energy away from or toward the blade row ($d_n^2 < 0$). The disturbance which shows growth with increasing axial distance from the blade row or propagation of energy toward the blade row must be eliminated. The condition $d_n^2 = 0$ which divides these two types of behavior is called the acoustic resonance or “cut-off”

condition. Here, the second term on the right-hand-side of (3.6) must be eliminated because the unsteady potential must remain bounded with increasing distance from the blade row. Thus in each case, $d_n^2 > 0$, $d_n^2 < 0$ or $d_n^2 = 0$, we can write

$$\phi_n^P(\xi, \eta) = a_n \exp[(h_n d_n + iM^2 \delta_n \cos \Omega) \xi + ik_{\eta, n} \eta] , \quad (3.9)$$

and our task is to determine the correct value of h_n (i.e., +1 or -1) for $d_n^2 \neq 0$.

It follows from (3.7) and some algebra that the circumferential wave numbers at which resonance occurs, $k_{\eta}^{(\pm)}$, are given by

$$k_{\eta}^{(\pm)} = \omega V^{-1} M (1 - M^2)^{-1} (M \sin \Omega \pm \sqrt{1 - M^2 \cos^2 \Omega}) , \quad M \neq 1 . \quad (3.10)$$

Note that $|M \sin \Omega| \leq (1 - M^2 \cos^2 \Omega)^{1/2}$ for $M \leq 1$. Also, the ranges of circumferential wave numbers for which disturbances vary exponentially in the axial direction (i.e., $d_n^2 > 0$) are given by

$$k_{\eta, n} < k_{\eta}^{(\mp)} \quad \text{for } M < 1 \quad \text{and } \omega \gtrless 0 , \quad (3.11a)$$

$$k_{\eta, n} > k_{\eta}^{(\pm)} \quad \text{for } M < 1 \quad \text{and } \omega \gtrless 0 \quad (3.11b)$$

and

$$k_{\eta}^{(\pm)} < k_{\eta, n} < k_{\eta}^{(\mp)} \quad \text{for } M > 1 \quad \text{and } \omega \gtrless 0 . \quad (3.12)$$

Those for which disturbances propagate in the axial direction (i.e., $d_n^2 < 0$) are given by

$$k_{\eta}^{(\mp)} < k_{\eta, n} < k_{\eta}^{(\pm)} \quad \text{for } M < 1 \quad \text{and } \omega \gtrless 0 , \quad (3.13)$$

$$k_{\eta, n} > k_{\eta}^{(\mp)} \quad \text{for } M > 1 \quad \text{and } \omega \gtrless 0 \quad (3.14a)$$

and

$$k_{\eta, n} < k_{\eta}^{(\pm)} \quad \text{for } M > 1 \quad \text{and } \omega \gtrless 0 . \quad (3.14b)$$

In the transonic limit ($M \rightarrow 1$) we find that

$$\lim_{M \rightarrow 1} k_{\eta}^{(\pm)} \rightarrow \begin{cases} 2\omega V^{-1} M^2 \sin \Omega / (1 - M^2) + \omega V^{-1} / (2 \sin \Omega) , & \Omega \leq 0 \\ -\omega V^{-1} / (2 \sin \Omega) , & \Omega \geq 0 \end{cases} \quad (3.15)$$

and the results achieved using the present analysis will agree with those based on a similar analysis of the high-frequency transonic small-disturbance equation (i.e., (2.8) with $A_{\mp\infty}$ set equal to $V_{\mp\infty}$). The high-frequency transonic equation (Landahl 1961) yields only a single resonant circumferential wave number, i.e., $k_{\eta}^{(M=1)} = -\omega V^{-1} / (2 \sin \Omega)$, and disturbances at circumferential wave numbers to one side of this resonant wave number are of propagating type while those at circumferential wave numbers to the other side are of decaying type.

It is a simple matter to determine the appropriate form of the fundamental solution for tangential wave numbers satisfying the inequalities in (3.11) and (3.12). Since physically admissible solutions must be bounded in the far field, h_n must be positive in the far upstream region ($\xi < \xi_-$) and negative in the far downstream region ($\xi > \xi_+$). For tangential wave numbers satisfying the inequalities in (3.13) and (3.14) the fundamental solution (3.9) describes a wave that propagates in the axial-flow direction at wave number

$$k_{\xi,n} = h_n |d_n| + M^2 \delta_n \cos \Omega \quad (3.16)$$

and the determination of the correct value of h_n is somewhat more difficult. Various methods have been proposed to dictate this choice. These involve adding an artificial damping term ($\epsilon_d \tilde{\phi}_t$) to the left-hand-side of the far-field differential equation (2.8) (Verdon, Adamczyk & Caspar 1975; Adamczyk 1978), considering an unsteady excitation with slowly growing temporal amplitude, i.e., with $\omega = \omega' - i\lambda$, where λ is a small positive number (Ni 1979), or determining a far-field solution in terms of coordinates moving at the uniform inlet or exit velocity (Whitehead & Davies 1983). In the first two methods the correct form of the fundamental solution is determined by requiring that the unsteady potential remains bounded as $|\xi| \rightarrow \infty$. Once this form is determined, ϵ_d or λ are allowed to approach zero. In the method of Whitehead & Davies (1983) the form of the fundamental solution in the moving coordinate frame which ensures that acoustic energy propagates away from the blade row is used to determine the correct value of h_n in (3.9) or (3.16). This method seems to have the most physical appeal and is therefore the one adopted herein.

Consider coordinate axes ξ' and η' parallel to the space-fixed ξ - and η -axes, respectively, but moving at the velocity \vec{V} . After replacing $\phi(\vec{X})$ by $\tilde{\phi}(\vec{X}, t) = \phi(\vec{X})e^{i\omega t}$ and $i\omega$ by $\partial/\partial t$ in the far-field equation (2.8) and applying the independent variable transformation

$$\xi' = \xi - V_\xi t, \quad \eta' = \eta - V_\eta t \quad \text{and} \quad t' = t \quad (3.17)$$

we find that

$$\tilde{\phi}_{\xi'\xi'} + \tilde{\phi}_{\eta'\eta'} - A^{-2} \tilde{\phi}_{t't'} = 0. \quad (3.18)$$

Equation (3.18) has a fundamental solution of the form

$$\tilde{\phi}(\vec{X}', t') = F(\vec{X}' \cdot \vec{e}_p - At') + G(\vec{X}' \cdot \vec{e}_p + At'), \quad (3.19)$$

where \vec{X}' is a position vector in the ξ', η' -coordinate frame and \vec{e}_p is a unit vector pointing in the direction of wave propagation. Since only those waves which propagate away from the blade row are admissible, $\vec{e}_p \cdot \vec{e}_\xi$ must be less than zero for $\xi' \rightarrow -\infty$ and greater than zero for $\xi' \rightarrow \infty$. Then, since the function G describes waves that propagate toward the blade row, it must be set equal to zero, and the nth term of the general solution to (3.18) can be written as

$$\tilde{\phi}_n(\xi', \eta', t') = b'_n \exp[i\omega'_n(t' - \xi' \cos \theta_n/A - \eta' \sin \theta_n/A)]. \quad (3.20)$$

This solution describes a wave propagating at speed A and at angle θ_n , measured counterclockwise from the ξ' -axis, where $\pi/2 < \theta_n < 3\pi/2$ for $\xi' \rightarrow -\infty$ and $|\theta_n| < \pi/2$ for $\xi' \rightarrow \infty$. The temporal frequency of the n th disturbance wave as seen by an observer moving with the mean fluid velocity \vec{V} is ω'_n .

A comparison of the result in (3.20) with the fundamental solution for $d_n^2 < 0$ in (3.9) dictates the correct value of h_n to be used in the latter equation. It follows from (3.7), (3.9), (3.16), and (3.20) that

$$\begin{aligned}\omega'_n &= \omega + \vec{k}_n \cdot \vec{V} = V(\delta_n + h_n | d_n | \cos \Omega) , \\ \omega'_n A^{-1} \sin \theta_n &= -k_{\eta,n}\end{aligned}$$

and

$$\omega'_n A^{-1} \cos \theta_n = -k_{\xi,n} , \quad (3.21)$$

where $k_{\eta,n}$ satisfies one of the inequalities in (3.13) and (3.14). Now, a disturbance carried by the n th wave travels in the axial direction with velocity $C_{\xi,n}$, where

$$C_{\xi,n} = V_\xi + A \cos \theta_n = -h_n A^2 (1 - M^2 \cos^2 \Omega) | d_n | / \omega'_n . \quad (3.22)$$

The right-hand-side of (3.22) follows from (3.16) and (3.21). Note that in the limit as $d_n^2 \rightarrow 0$ (i.e., as a resonance condition is approached), $C_{\xi,n} \rightarrow 0$ and there is no transfer of acoustic energy in the axial direction. Since the velocity $C_{\xi,n}$ must be less than zero in the far upstream region and greater than zero in the far downstream region, the correct value of h_n in (3.16), (3.21) and (3.22) depends on the sign of ω'_n . Some analysis of (3.7), (3.8), (3.13) and (3.14) shows that $\delta_n \gtrless \pm |d_n| \cos \Omega$ for $\omega \gtrless 0$ if the free-stream flow is subsonic and $k_\eta^{(\mp)} < k_{\eta,n} < k_\eta^{(\pm)}$, or if the free-stream flow is supersonic with the product $\omega \Omega > 0$ and $k_{\eta,n} > k_\eta^{(\mp)}$ or with $\omega \Omega < 0$ and $k_{\eta,n} < k_\eta^{(\pm)}$. Under these conditions ω'_n and ω have the same sign; therefore, $h_n = \text{sgn}(\omega)$ in the far upstream ($\xi < \xi_-$) region and $h_n = -\text{sgn}(\omega)$ in the far downstream ($\xi > \xi_+$) region, where $\text{sgn}(\omega) = \pm 1$ for $\omega \gtrless 0$. If the free-stream flow is supersonic with $\omega \Omega > 0$ and $k_{\eta,n} < k_\eta^{(\pm)}$ or with $\omega \Omega < 0$ and $k_{\eta,n} > k_\eta^{(\mp)}$, then $\delta_n \gtrless \mp |d_n| \cos \Omega$ for $\omega \gtrless 0$. In this case ω'_n and ω are of opposite sign and $h_n = \mp \text{sgn}(\omega)$ for $\xi \gtrless \xi_\mp$.

Thus, as a result of the foregoing analysis, we can write the solution for the unsteady potential in the far field due to the acoustic response fluctuations as

$$\phi^P(\vec{X}) = \sum_{n=-\infty}^{\infty} a_{n,\mp\infty} \exp[\chi_n(\xi - \xi_\mp) + i k_{\eta,n}(\eta - \eta_\mp)], \quad \xi \gtrless \xi_\mp . \quad (3.23)$$

The constants $a_{n,\mp\infty}$ are determined by matching these analytic solutions to a near-field (numerical) solution, (ξ_-, η_-) and (ξ_+, η_+) are reference locations, i.e., the points of intersection of the reference blade ($m = 0$) stagnation streamline and the lines $\xi = \xi_-$

and $\xi = \xi_+$, respectively, and

$$\chi_n = \beta_n + ik_{\xi,n} = \left\{ \begin{array}{l} \pm |d_n| + iM^2\delta_n \cos \Omega \\ i(\pm \text{sgn}(\omega) |d_n| + M^2\delta_n \cos \Omega) \\ i(\mp \text{sgn}(\omega) |d_n| + M^2\delta_n \cos \Omega) \end{array} \right\} \quad \text{for } \xi < \xi_+, \quad (3.24a)$$

$$i(\pm \text{sgn}(\omega) |d_n| + M^2\delta_n \cos \Omega) \quad (3.24b)$$

$$i(\mp \text{sgn}(\omega) |d_n| + M^2\delta_n \cos \Omega) \quad (3.24c)$$

where d_n and δ_n are defined in (3.7) and (3.8). At resonance (i.e., $k_{\eta,n} = k_n^{(\pm)}$ (see (3.10))) $|d_n| = 0$. If $|d_n| \neq 0$, χ_n is determined using (3.24a) if the inequalities in (3.11a), (3.11b) or (3.12) are satisfied; (3.24b) if the inequalities in (3.13), (3.14a) for $\omega\Omega > 0$ or (3.14b) for $\omega\Omega < 0$ are satisfied; and (3.24c) if the inequalities in (3.14b) for $\omega\Omega > 0$ or in (3.14a) for $\omega\Omega < 0$ are satisfied. This information is summarized in figures 2 and 3. In the limit $M \rightarrow 1$ the subsonic (see figure 2) and supersonic (figure 3) results become identical, and therefore no disturbances of the type 3.24c can exist in a transonic free stream. It is also important to note that the expression for the potential due to prescribed far upstream and/or far downstream acoustic excitations must have the same form as (3.23) except that the χ_n must be replaced by $-\chi_n$.

An analysis similar to the above can be performed for supersonic relative flow with supersonic axial velocity component (see also Ni 1979; Whitehead 1987). In this case the fundamental solutions for ϕ^P are also given by (3.5), (3.6) and (3.7), but d_n^2 is less than zero for all circumferential wave numbers. Therefore each fundamental solution describes two propagating acoustic response disturbances. It is easy to show that both of these disturbances carry energy in the downstream axial direction. Hence, for supersonic streams with $M \cos \Omega > 1$ the potential ϕ^P due to acoustic response disturbances has the form

$$\phi^P(\vec{X}) = \left\{ \begin{array}{ll} 0 & , \quad \xi < \xi_- \\ \sum_{n=-\infty}^{\infty} \{a_{1,n} \exp[\chi_{1,n}(\xi - \xi_+)] + a_{2,n} \exp[\chi_{2,n}(\xi - \xi_+)]\} \\ \times \exp[ik_{\eta,n}(\eta - \eta_+)] & , \quad \xi > \xi_+ \end{array} \right. \quad (3.25a)$$

$$(3.25b)$$

where $\chi_{1,n}$ and $\chi_{2,n}$ are defined by (3.7) and (3.8).

In a supersonic stream with supersonic axial velocity component only far upstream acoustic excitations can affect the flow through the blade row. The potential due to such excitations has the same form as (3.25b), except that ξ_+ and η_+ must be replaced by ξ_- and η_- , respectively. Because of the manner in which unsteady disturbances propagate in supersonic streams, an analytic solution for the velocity potential response in the far upstream or far downstream region is not required to determine the unsteady flow through a cascade operating at supersonic inlet or exit velocity. Thus, our concern here is primarily with cascades operating at subsonic axial inlet and exit velocities for which a knowledge of the far-field potential response is indeed required to predict near field unsteady flows. Hence, throughout the remainder of this report when we refer to supersonic inlet or exit conditions, it is assumed implicitly that the axial velocity component is subsonic.

4. THE UNSTEADY POTENTIAL DUE TO VORTICAL DISTURBANCES

The unsteady potential component ϕ^R is determined as a solution of the differential equations (3.2) and (3.3) which satisfies cascade periodicity (2.4) and the conditions of continuity of pressure (2.10) and normal velocity component (2.11) across blade wakes. In one sense it is a much simpler task to determine ϕ^R than it is to determine the far-field potential ϕ^P because a single expression holds for ϕ^R regardless of the sign of $M - 1$, $M \cos \Omega - 1$, Ω or ω . However, the potential component ϕ^R depends upon the rotational velocity fluctuation and therefore, we must first determine a solution for $\vec{v}^R(\xi > \xi_+, \eta)$ before proceeding to determine the corresponding solution for ϕ^R .

4.1 The Rotational Velocity in the Far Downstream Region

The rotational velocity in the far downstream region is determined as a solution to the field equation (2.9) for a periodic (in η) distribution of rotational velocity along $\xi = \xi_+$ which can, in general, be discontinuous at blade wakes. To determine this solution it is again convenient to decompose the dependent variable into two components. Thus we set

$$\vec{v}^R = \vec{v}_c^R + \vec{v}_d^R, \quad (4.1)$$

where \vec{v}_c^R is continuous and \vec{v}_d^R possesses jump discontinuities at blade wakes, i.e.,

$$[\vec{v}_d^R] = [\vec{v}^R]_{Ref} \exp[i(m\sigma - \omega V_\infty^{-1} T_m)] \quad \text{on } W_m, \quad m = 0, \pm 1, \pm 2, \dots . \quad (4.2)$$

We require that both \vec{v}_c^R and \vec{v}_d^R satisfy (2.9) and the periodicity condition (2.4) and that $\nabla \cdot \vec{v}_d^R = 0$. It then follows from (2.9) and (2.4) that

$$\vec{v}_c^R = \sum_{n=-\infty}^{\infty} \vec{b}_n \exp[i \vec{k}_n \cdot (\vec{X} - \vec{X}_+)], \quad \xi \geq \xi_+, \quad (4.3)$$

where the Fourier coefficients, \vec{b}_n , are determined in terms of the rotational velocity distribution on $\xi = \xi_+$ (see (4.24) below) and

$$\begin{aligned} \vec{k}_n &= -(\omega V_\infty^{-1} \sec \Omega_\infty + k_{\eta,n} \tan \Omega_\infty) \vec{e}_\xi + k_{\eta,n} \vec{e}_\eta \\ &= -\omega V_\infty^{-1} \vec{e}_T + (\omega V_\infty^{-1} \tan \Omega_\infty + k_{\eta,n} \sec \Omega_\infty) \vec{e}_N, \end{aligned} \quad (4.4)$$

where $k_{\eta,n} = (\sigma + 2\pi n)G^{-1}$.

A particular solution for the discontinuous component of the rotational velocity, \vec{v}_d^R , in the far downstream region of the m th passage (i.e., in the region $T_m > 0$, $0 < N_m < G \cos \Omega_\infty$) can be determined conveniently in terms of the Cartesian coordinates T_m and N_m . Once this result is obtained, it can be extended to provide a solution in terms of the independent variables ξ and η which holds over the entire downstream

region. It follows from (2.9) and (4.2) that the required solution for the m th passage can be written in the form

$$\vec{v}_d^R = \vec{F}_m(N_m) \exp(-i\omega V_\infty^{-1} T_m). \quad (4.5)$$

Since \vec{v}_d^R is divergence free and has a jump discontinuity across blade wakes,

$$-i\omega V_\infty^{-1} \vec{F}_m \cdot \vec{e}_T + \vec{F}_m' \cdot \vec{e}_N = 0 \quad (4.6)$$

and

$$\vec{F}_m(0^+) - \vec{F}_m(G \cos \Omega^-) \exp[-i(\sigma + \omega V_\infty^{-1} G \sin \Omega)] = [\vec{v}]_{Ref}^R \exp(im\sigma), \quad (4.7)$$

respectively. A solution for \vec{F}_m which meets the requirements (4.6) and (4.7) can be constructed as a linear combination of the exponential functions $\exp(\omega V_\infty^{-1} N_m)$ and $\exp(-\omega V_\infty^{-1} N_m)$. After making several trials and performing some algebra, we find that

$$\begin{aligned} \vec{F}_m(N_m) &= e^{im\sigma} [C_1 \exp(\omega V_\infty^{-1} N_m) (\vec{e}_T + i \vec{e}_N) \\ &\quad + C_2 \exp(-\omega V_\infty^{-1} N_m) (\vec{e}_T - i \vec{e}_N)], \end{aligned} \quad (4.8)$$

where the constants C_1 and C_2 are given by

$$C_1 = \frac{1}{2} [1 - \exp(\omega V_\infty^{-1} G e^{-i\Omega_\infty} - i\sigma)] [\vec{v}]_{Ref}^R \cdot (\vec{e}_T - i \vec{e}_N) \quad (4.9a)$$

and

$$C_2 = \frac{1}{2} [1 - \exp(-\omega V_\infty^{-1} G e^{i\Omega_\infty} - i\sigma)] [\vec{v}]_{Ref}^R \cdot (\vec{e}_T + i \vec{e}_N). \quad (4.9b)$$

The solution for the rotational velocity over the entire far downstream region ($\xi > \xi_+$) is then determined by combining the results in (4.1), (4.3), (4.5), (4.8) and (4.9) to obtain

$$\begin{aligned} \vec{v}^R(\vec{X}) &= \sum_{n=-\infty}^{\infty} \vec{b}_n \exp[i \vec{k}_n \cdot (\vec{X} - \vec{X}_+)] \\ &\quad + C_1 \exp[-i\omega V_\infty^{-1}(\vec{X} - \vec{X}_+) \cdot (\vec{e}_\xi + i \vec{e}_\eta) e^{-i\Omega_\infty}] (\vec{e}_\xi + i \vec{e}_\eta) e^{-i\Omega_\infty} \\ &\quad \times \sum_{m=-\infty}^{\infty} \exp[im\sigma - m\omega V_\infty^{-1} G e^{-i\Omega_\infty}] [U(\eta - \eta_{w_m}) - U(\eta - \eta_{w_{m+1}})] \\ &\quad + C_2 \exp[-i\omega V_\infty^{-1}(\vec{X} - \vec{X}_+) \cdot (\vec{e}_\xi - i \vec{e}_\eta) e^{i\Omega_\infty}] (\vec{e}_\xi - i \vec{e}_\eta) e^{i\Omega_\infty} \\ &\quad \times \sum_{m=-\infty}^{\infty} \exp[im\sigma + m\omega V_\infty^{-1} G e^{i\Omega_\infty}] [U(\eta - \eta_{w_m}) - U(\eta - \eta_{w_{m+1}})]. \end{aligned} \quad (4.10)$$

Here

$$\eta = \eta_{w_m} = \eta_+ + mG + (\xi - \xi_+) \tan \Omega_\infty \quad (4.11)$$

defines the location of the straight-line approximation to the m th wake,

$$\begin{aligned} \vec{X} - \vec{X}_+ &= (\xi - \xi_+) \vec{e}_\xi + (\eta - \eta_+) \vec{e}_\eta \\ &= (T_m + mG \sin \Omega_\infty) \vec{e}_T + (N_m + mG \cos \Omega_\infty) \vec{e}_N \end{aligned} \quad (4.12)$$

and

$$\vec{e}_\xi \pm i \vec{e}_\eta = (\vec{e}_T \pm i \vec{e}_N) \exp(\pm i \Omega_\infty). \quad (4.13)$$

The divergence of the rotational velocity in the far downstream region is given by

$$\nabla \cdot \vec{v}^R = \sum_{n=-\infty}^{\infty} i \vec{k}_n \cdot \vec{b}_n \exp[i \vec{k}_n \cdot (\vec{X} - \vec{X}_+)]. \quad (4.14)$$

4.2 The Potential due to Vortical Disturbances

As in the case of the rotational velocity, we seek first a solution for the potential component ϕ^R in the far downstream region of the m th passage (i.e., $T_m > 0, 0 < N_m < G \cos \Omega$) and then extend this result to provide a solution over the entire far downstream region ($\xi > \xi_+$). It follows from the field equations (3.2) and (3.3), the cascade periodicity (2.4) and wake-jump conditions (2.10) and (2.11), and the foregoing results for the far downstream rotational velocity that the required solution must be of the form

$$\phi^R(T_m, N_m) = H_m(N_m) \exp(-i\omega V_\infty^{-1} T_m), \quad (4.15)$$

where

$$H_m''(N_m) - \omega^2 V_\infty^{-2} H(N_m) = - \sum_{n=-\infty}^{\infty} i \vec{k}_n \cdot \vec{b}_n \exp\{i[k_{N,n} N_m + m(\sigma + 2\pi n)]\}, \quad (4.16)$$

$$H_m(0^+) - \exp[-i(\sigma + \omega V_\infty^{-1} G \sin \Omega_\infty)] H(G \cos \Omega_\infty^-) = [\phi]_{Ref} \exp(im\sigma) \quad (4.17)$$

and

$$H'_m(0^+) - \exp[-i(\sigma + \omega V_\infty^{-1} G \sin \Omega_\infty)] H'(G \cos \Omega_\infty^-) = -[\vec{v}^R]_{Ref} \cdot \vec{e}_N \exp(im\sigma). \quad (4.18)$$

The general solution of (4.16) is

$$\begin{aligned} H_m(N_m) &= D_1 \exp(im\sigma) \exp(\omega V_\infty^{-1} N_m) + D_2 \exp(im\sigma) \exp(-\omega V_\infty^{-1} N_m) \\ &\quad + \sum_{n=-\infty}^{\infty} \frac{i \vec{k}_n \cdot \vec{b}_n}{|\vec{k}_n|^2} \exp\{i[k_{N,n} N_m + m(\sigma + 2\pi n)]\}. \end{aligned} \quad (4.19)$$

The constants D_1 and D_2 are evaluated using the wake conditions (4.17) and (4.18) and are given by

$$D_1 = \frac{1}{2} [1 - \exp(-i\sigma + \omega V_\infty^{-1} G e^{-i\Omega_\infty})]^{-1} (\llbracket \phi \rrbracket_{Ref} - \omega^{-1} V_\infty^{-1} \llbracket \vec{v}^R \rrbracket_{Ref} \cdot \vec{e}_N) \quad (4.20a)$$

and

$$D_2 = \frac{1}{2} [1 - \exp(-i\sigma - \omega V_\infty^{-1} G e^{i\Omega_\infty})]^{-1} (\llbracket \phi \rrbracket_{Ref} + \omega^{-1} V_\infty \llbracket \vec{v}^R \rrbracket_{Ref} \cdot \vec{e}_N). \quad (4.20b)$$

Therefore, the solution for the velocity potential fluctuations in the far downstream region of the m th passage due to rotational velocity disturbances and wake vorticity, is given by

$$\begin{aligned} \phi^R(T_m, N_m) &= e^{im\sigma} \{ D_1 \exp[-i\omega V_\infty^{-1}(T_m + iN_m)] + D_2 \exp[-i\omega V_\infty^{-1}(T_m - iN_m)] \} \\ &+ \sum_{n=-\infty}^{\infty} \frac{i \vec{k}_n \cdot \vec{b}_n}{|\vec{k}_n|^2} \exp\{i[k_{T,n} T_m + k_{N,n} N_m + m(\sigma + 2n\pi)]\} \end{aligned} \quad (4.21)$$

Finally, the solution for ϕ^R over the entire downstream region $\xi > \xi_+$ is

$$\begin{aligned} \phi^R(\vec{X}) &= D_1 \exp[-i\omega V_\infty^{-1}(\vec{X} - \vec{X}_+) \cdot (\vec{e}_\xi + i \vec{e}_\eta) e^{-i\Omega_\infty}] \\ &\times \sum_{m=-\infty}^{\infty} \exp[im\sigma - \omega V_\infty^{-1} m G e^{-i\Omega_\infty}] [U(\eta - \eta_{W_m}) - U(\eta - \eta_{W_{m+1}})] \\ &+ D_2 \exp[-i\omega V_\infty^{-1}(\vec{X} - \vec{X}_+) \cdot (\vec{e}_\xi - i \vec{e}_\eta) e^{i\Omega_\infty}] \\ &\times \sum_{m=-\infty}^{\infty} \exp[im\sigma + \omega V_\infty^{-1} m G e^{i\Omega_\infty}] [U(\eta - \eta_{W_m}) - U(\eta - \eta_{W_{m+1}})] \\ &+ \sum_{n=-\infty}^{\infty} \frac{i \vec{k}_n \cdot \vec{b}_n}{|\vec{k}_n|^2} \exp[i \vec{k}_n \cdot (\vec{X} - \vec{X}_+)]. \end{aligned} \quad (4.22)$$

4.3 The Complete Solution for the Unsteady Potential

We have considered the flow through an isolated two-dimensional blade row in which unsteady fluctuations are produced by small-amplitude periodic (in η and t) structural (blade motions) and/or external aerodynamic excitations (incident entropic, vortical or acoustic disturbances). Far from the blade row the complex amplitude, $\phi(\vec{X})$, of the linearized unsteady potential can be expressed as the sum of two components (3.1)—one, $\phi^P(\vec{X})$, associated with acoustic disturbances and the other, $\phi^R(\vec{X})$, associated with vortical disturbances. Analytic solutions for ϕ^P and ϕ^R due to acoustic and vortical response fluctuations are given in (3.23) for subsonic axial flow and (4.22),

respectively. The unsteady potential component ϕ^R depends upon the far downstream rotational velocity field which is described in (4.10).

The physical variables that the potential component ϕ^P depends on explicitly are the free-stream Mach number and flow angle, the cascade blade spacing, the frequency and interblade phase angle of the unsteady excitation and the complex amplitudes of the first-harmonic acoustic disturbances. In particular, the complex amplitudes, $a_{n,\mp\infty}$, of the acoustic response fluctuations are given by

$$a_{n,\mp\infty} = G^{-1} \int_{\eta_\mp}^{\eta_\mp+G} [\phi(\xi_-, \eta) - \phi^R(\xi_+, \eta) U(\xi - \xi_+)] \exp(-ik_{n,n}\eta) d\eta . \quad (4.23)$$

Note that if a trailing-edge Kutta condition is imposed to determine the steady flow through the blade row, the exit free-stream conditions cannot be prescribed arbitrarily, but are determined by the conditions imposed at the cascade inlet. The physical variables that the potential component ϕ^R depends on are the far downstream free-stream flow speed and angle, the blade spacing, the frequency and interblade phase angle of the unsteady excitation, the complex amplitudes of the rotational velocity fluctuations, \vec{b}_n , where

$$\vec{b}_n = G^{-1} \int_{\eta_+}^{\eta_++G} [\vec{v}^R(\xi_+, \eta) - \vec{v}_d^R(\xi_+, \eta)] \exp(-ik_{n,n}\eta) d\eta , \quad (4.24)$$

and the jumps in the potential $[\phi]_{Ref}$ and rotational velocity $[\vec{v}^R]_{Ref}$ at the intersection of the reference wake and the axial line $\xi = \xi_+$. Note that if the rotational velocity is continuous across blade wakes, the constants C_1 and C_2 in (4.10) are identically zero and the constants D_1 and D_2 in (4.22) depend only on the jump in potential $[\phi]_{Ref}$. In addition, if there are no prescribed incident rotational velocity disturbances, $\vec{v}^R(\bar{X}) \equiv 0$ throughout the field and the last term in (4.22) is identically zero. In this important special case ϕ^R is driven only by the vorticity shed at the blade trailing edges and convected along the blade wakes, which is directly related to the fluctuating aerodynamic loads acting on the blades.

4.4 Implementation of Far-Field Solutions in Numerical Computations

The complex amplitudes $a_{n,\mp\infty}$ and \vec{b}_n , the potential and rotational velocity jumps $[\phi]_{Ref}$ and $[\vec{v}^R]_{Ref}$, and hence, the far-field solutions for ϕ and \vec{v}^R are known in terms of the potential distributions along the lines $\xi = \xi_\mp$ and the rotational velocity distribution along $\xi = \xi_+$. This feature can be applied to construct a discrete approximation to the linearized unsteady boundary-value problem over an extended blade passage region bounded by the axial lines $\xi = \xi_\mp$. For example, if the computational mesh consists of one set of lines parallel to the blade row (see Verdon & Caspar 1982, 1984), then the discrete approximation to the field equation (2.8) at mesh points on the boundary lines $\xi = \xi_\mp$ will depend upon values of ϕ and \vec{v}^R upstream and downstream, respectively, of these axial mesh lines. However, because the potential upstream of $\xi = \xi_-$ and the

potential and rotational velocity downstream of $\xi = \xi_+$ are known (see (3.23), (4.10) and (4.22)) in terms of the potential distribution on $\xi = \xi_-$ and the potential and rotational velocity distributions on $\xi = \xi_+$, the discrete approximations to the field equations on $\xi = \xi_{\mp}$ can be constructed entirely in terms of ϕ and \vec{v}^R values at points on the upstream and downstream boundaries and in the interior ($\xi_- < \xi < \xi_+$) of the computational domain. Thus, using the analytic far-field solutions, we can write a discrete equation for each unknown ϕ value which depends only upon information within and on the boundaries of the computational domain. Hence, the system of discrete equations is completely specified.

The foregoing approach has been used in the blade flutter calculations ($s = \vec{v}^R = p_I = 0$) (see Whitehead 1982; Verdon & Caspar 1982, 1984; Usab & Verdon 1986) and is a particularly convenient one for cascades operating under subsonic inlet and exit conditions because only a limited number of acoustic response waves persist in the far field. For supersonic flows with subsonic axial velocity component, the Fourier series representation for ϕ^P (3.23) may not be so useful because, in principle, many terms of this series will be needed to represent the abrupt changes in the velocity potential that occur at Mach waves. We should also note that, in addition to their use in constructing complete sets of finite-difference equations, the understanding of the unsteady flow in the far field gained through an examination of the analytic far-field solutions is essential to an accurate resolution of the flow through the cascade. In particular, mesh spacings must be selected so that the important variations in the rotational velocity and the velocity potential, indicated by the unsteady flow behavior in the far field, can be resolved accurately.

5. UNSTEADY FLOW BEHAVIOR IN THE FAR FIELD

We proceed to analyze the unsteady aerodynamic response in the far field of an isolated two-dimensional cascade operating at subsonic axial inlet and exit velocity by examining the parametric dependence of the wave numbers and attenuation constants, that control the spatial variation of far-field potential disturbances. This type of information is a prerequisite for prescribing the computational mesh needed for a numerical resolution of the unsteady flow through the blade row. Thus we will examine the behavior of the velocity potential in the far upstream and downstream regions caused by acoustic response disturbances and the behavior of the potential in the far downstream region caused by continuous rotational velocity disturbances and concentrated vorticity convected along the blade wakes. But first we will provide a useful classification for unsteady excitations which is based upon the acoustic responses that they produce in the far field.

5.1 Classification of Unsteady Excitations

We consider a fundamental pressure response disturbance and using (3.10) define the constant C_n as

$$C_n = \frac{|\omega| M (1 - M^2 \cos^2 \Omega)^{\frac{1}{2}}}{|(1 - M^2)V k_{\eta,n} - \omega M^2 \sin \Omega|} \quad (5.1)$$

where the subscripts $-\infty$ or $+\infty$ must be applied to M , V and Ω and therefore C_n to refer to the far upstream or far downstream flow regions. We then classify the nth pressure response disturbance as subresonant, resonant or superresonant depending upon whether C_n is less than, equal to, or greater than one, respectively (see also Samoilovich 1967; Verdon 1979; Bendiksen 1986). For a prescribed Mach number, flow angle and excitation frequency, resonance ($C_n = 1$) occurs at two different circumferential wave numbers, i.e., $k_{\eta}^{(\mp)}$. The nth acoustic response disturbance is superresonant ($C_n > 1$) for circumferential wave numbers lying between these two resonant values (see (3.12) and (3.13)) and subresonant ($C_n < 1$) for circumferential wave numbers less than the lower and greater than the higher of the two resonant circumferential wave numbers (see (3.11) and (3.14)). This information is also illustrated in figures 2 and 3.

For subsonic ($M < 1$) relative flow $k_{\eta}^{(-)}$ and $k_{\eta}^{(+)}$ have different signs. Thus one resonance condition (i.e., $k_{\eta}^{(\pm)}$ for $\omega \gtrless 0$) corresponds to a response disturbance travelling in the positive η -direction and the other (i.e., $k_{\eta}^{(\mp)}$ for $\omega \gtrless 0$) to a wave traveling in the negative η -direction. In a subsonic free stream subresonant disturbances attenuate with increasing distance from the blade row (i.e., χ_n is determined using (3.24a)) while superresonant disturbances propagate away from the blade row (χ_n is determined using (3.24b)). It follows from (5.1) that C_n can be greater than one only for a limited number of acoustic response fluctuations and hence, in subsonic flow, that such fluctuations must be either all or mostly all of decaying type.

For supersonic flow with subsonic axial velocity component both resonant circumferential wave numbers describe waves traveling in the same direction, i.e., the negative

η -direction if both ω and Ω have the same sign and the positive η -direction if ω and Ω differ in sign. In a supersonic free-stream superresonant disturbances attenuate with increasing axial distance from the blade row (i.e., χ_n is determined using (3.24a)), while subresonant disturbances propagate and carry energy away from the blade row (χ_n is determined using (3.24b) or (3.24c)). Since C_n can be greater than one only for a limited number of acoustic response disturbances, the latter are either all or mostly all of propagating type.

We can classify unsteady excitations based on the acoustic response that they produce in the far field as follows. Recall that the far upstream and far downstream free-stream conditions will generally differ. Indeed, the flow may be subsonic in one far-field region and supersonic in the other. We refer to an unsteady excitation as subresonant if it produces only acoustic response disturbances which attenuate with increasing distance from the blade row at subsonic free-stream Mach numbers or only disturbances which persist and carry energy away from the blade row at supersonic free-stream Mach numbers. A resonant excitation is one for which at least one response wave persists and carries energy parallel to the blade row in either the far upstream or far downstream region regardless of whether the free-stream Mach numbers are subsonic or supersonic. Finally, a superresonant (m,n) excitation is one for which m,n waves persist and carry energy away from the blade row at subsonic inlet, exit Mach numbers or attenuate with increasing distance from the blade row at supersonic inlet, exit Mach numbers. Note that if either m or n , but not both, is zero, the excitation is regarded as superresonant. Thus, if the inlet and exit Mach numbers are both subsonic, an excitation classified as superresonant $(1,0)$ produces one wave which carries energy away from the blade row in the upstream axial direction, but all other acoustic response disturbances associated with this excitation attenuate with increasing axial distance from the blade row.

5.2 The Acoustic Response in the Far Field

To illustrate the acoustic response in the far field in more detail we introduce the scaled variables

$$\ell_\eta = \omega^{-1} V k_{\eta,n} = V \omega^{-1} G^{-1} (\sigma + 2\pi n), \quad (5.2)$$

$$\ell_\xi = \omega^{-1} V \operatorname{Im}\{\chi_n\} \quad (5.3)$$

and

$$\bar{\beta} = \omega^{-1} V |\operatorname{Re}\{\chi_n\}| \quad (5.4)$$

where χ_n is defined in (3.24), $n = 0, 1, 2, \dots$, and we assume that the interblade phase angle of the unsteady excitation varies between $-\pi$ and $+\pi$, i.e., $\sigma \in [-\pi, \pi]$. The resonant values (i.e., $\ell_\eta^{(\pm)}$) of the scaled circumferential wave number depend upon the free-stream Mach number and flow angle (see 3.10), while the axial wave number, ℓ_ξ , and the attenuation constant, $\bar{\beta}$, can be expressed as functions of the free-stream Mach number, the free-stream flow angle and the tangential wave number (see (3.24) and (3.7)). Results illustrating the behavior of these parameters for selected subsonic

$(M < 1)$ flows and supersonic ($M > 1$) flows with subsonic axial velocity component ($M \cos \Omega < 1$) are presented below. Although these results depict ℓ_ξ and $\bar{\beta}$ as continuous functions of ℓ_η , it must be emphasized that a prescribed excitation at temporal frequency ω produces only a discrete set of acoustic response disturbances at $\ell_\eta = (\omega G)^{-1}V(\sigma + 2\pi n), n = 0, 1, 2, \dots$. Also, although upstream and downstream acoustic response properties are depicted below for the same free-stream Mach number and flow angle, the far upstream and far downstream free-stream states will generally differ.

The subsonic results and the supersonic resonance curves presented below hold for both positive and negative excitation frequencies ($\omega \gtrless 0$) and non-negative flow angles ($\Omega \geq 0$); the supersonic results for ℓ_ξ and $\bar{\beta}$ hold for $\omega > 0$ and $\Omega > 0$. Corresponding results for other combinations of ω and Ω can be readily determined from those provided here. Thus, resonance curves for $\Omega < 0$ are obtained by changing $\Omega, \ell_\eta^{(+)}, \ell_\eta^{(-)}$ and ℓ_η in figures 4 and 7 to $-\Omega, \ell_\eta^{(-)}, \ell_\eta^{(+)}$ and $-\ell_\eta$, respectively. Predictions of ℓ_ξ and $\bar{\beta}$ for $M < 1$ and $\Omega \leq 0$ and for $M > 1, \omega > 0$ and $\Omega < 0$ can be obtained from those given in figures 5, 6, 8 and 9 by changing ℓ_η to $-\ell_\eta$. Predictions of ℓ_ξ and $\bar{\beta}$ for $M > 1, \omega < 0$ and $\Omega > 0$ are obtained by changing $\ell_{\xi,-\infty}$ and $\ell_{\xi,\infty}$ to $\ell_{\xi,\infty}$ and $\ell_{\xi,-\infty}$, respectively, in figures 8 and 9. Finally predictions of ℓ_ξ and $\bar{\beta}$ for $M > 1, \omega < 0$ and $\Omega < 0$ are obtained by changing $\ell_\eta, \ell_{\xi,-\infty}$ and $\ell_{\xi,\infty}$ in figures 8 and 9 to $-\ell_\eta, \ell_{\xi,\infty}$ and $\ell_{\xi,-\infty}$, respectively.

5.2.1 Subsonic Flow

The resonant values of ℓ_η are plotted versus Mach number (as ordinate) for various free-stream flow angles in figure 4. The resonant circumferential wave number $\ell_\eta^{(+)}$ varies substantially with Mach number and flow angle, particularly at high subsonic Mach number, but, except at low flow angles, the dependence of $\ell_\eta^{(-)}$ on M and Ω is rather limited. Indeed, as $M \rightarrow 1$ from below, $\ell_\eta^{(+)} \rightarrow \infty$ and $\ell_\eta^{(-)} \rightarrow -(2 \sin \Omega)^{-1}$. As indicated in figure 4, the extent of the superresonant region or interval, i.e., $(\ell_\eta^{(-)}, \ell_\eta^{(+)})$, increases with increasing free-stream Mach number and to a lesser degree with increasing flow angle.

For example, consider an unsteady flow driven by a unit frequency excitation ($\omega = 1$) through a cascade with unit blade spacing ($G = 1$) and operating in a free stream with $V = 1$ and $\Omega = 45$ deg. These conditions are somewhat representative of those at which jet engine fan or compressor blades have experienced subsonic flutter. The calculations leading to the curve for $\Omega = 45$ deg in figure 4 indicate that for a free-stream Mach number of 0.7 and interblade phase angles lying in the range $[-\pi, \pi]$ all acoustic waves attenuate in the far field if the interblade phase angle, σ , of the unsteady excitation satisfies the conditions $\sigma < -0.513$ or $\sigma > 1.872$, but that one such wave (i.e., the $n = 0$ wave) will persist and carry energy away from the blade row if $-0.513 < \sigma < 1.872$. At a Mach number of 0.8 the corresponding ranges are $\sigma < -0.575$ or $\sigma > 3.09$ and $0.575 < \sigma < 3.09$, respectively. The situation becomes more interesting

at $M = 0.9$ where propagating waves occur for all values of σ . In particular, these waves occur at circumferential wave numbers $k_{\eta,n} = \sigma + 2\pi n$ lying in the range $(-0.639, 6.668)$. Both the $n = 0$ and $n = 1$ acoustic response disturbances persist in the far field if $-0.639 < \sigma < 0.385$, but only the $n = 1$ or the $n = 0$ disturbance persists if $-\pi < \sigma < -0.639$ or $0.385 < \sigma < \pi$, respectively. As the Mach number is increased further for our example configuration, additional acoustic response disturbances will be of propagating type. Note that in addition to the dependence on Mach number and flow angle indicated in figure 4, the extent of the range of circumferential wave numbers $(k_{\eta}^{(-)}, k_{\eta}^{(+)})$ for which acoustic response disturbances carry energy away from the blade row is directly proportional to the excitation frequency and inversely proportional to free-stream speed.

Curves illustrating the behavior of the axial wave number, ℓ_{ξ} , and attenuation constant, $\bar{\beta}$, for various subsonic free-stream Mach numbers and a free-stream flow angle of 45 deg are shown in figure 5. Curves for $M = 0.8$ and flow angles of 15 deg, 45 deg and 75 deg are shown in figure 6. The points on these curves at which $(\partial / \partial \ell_{\eta})|_{M,\Omega}$ are discontinuous are the resonant values of ℓ_{η} . For superresonant disturbances, $\ell_{\eta} \epsilon(\ell_{\eta}^{(-)}, \ell_{\eta}^{(+)})$, the far upstream and far downstream axial wave numbers differ and $\bar{\beta} = 0$. The difference $\ell_{\xi,-\infty} - \ell_{\xi,\infty}$ increases with increasing Mach number. For subresonant disturbances, $\ell_{\eta} \epsilon(-\infty, \ell_{\eta}^{(-)})$ or $\ell_{\eta} \epsilon(\ell_{\eta}^{(+)}, \infty)$, the far upstream and far downstream wave numbers are identical and depend linearly on ℓ_{η} . The attenuation constant $\bar{\beta}$ increases with $|\ell_{\eta}|$ and depends linearly on $|\ell_{\eta}|$ as $|\ell_{\eta}| \rightarrow \infty$. Thus, except at Mach numbers close to one, acoustic response disturbances of high wave-number magnitude attenuate rapidly with increasing distance from the blade row. This is an important feature which allows the successful application of numerical field methods to resolve unsteady flows through cascades operating at subsonic inlet and exit conditions.

To examine a typical situation in more detail we again consider the case $\omega = 1$, $G = 1$, $V = 1$, and $\Omega = 45$ deg. In addition, we consider an unsteady excitation at $\sigma = 0.5$. Such an excitation produces an ($n = 0$) acoustic response disturbance at $M = 0.7, 0.8$ and 0.9 which carries energy away from the blade row in both the far upstream and far downstream regions. The calculations used to determine the curves in figures 5 and 6 indicate that the axial wave numbers of the upstream propagating disturbance are 1.736, 2.373 and 3.245, respectively, and those for the downstream traveling disturbance are $-0.494, -0.572$ and -0.639 , respectively. The $n = \pm 1, \pm 2, \dots$ acoustic response fluctuations at $\ell_{\eta} = \sigma + 2\pi n$ attenuate with distance from the blade row and, except for the $n = 1$ disturbance at $M = 0.9$, they attenuate quite rapidly. The attenuation constant and axial wave number for the $n = 1$ disturbance (i.e., $\ell_{\eta} = k_{\eta,1} = \sigma + 2\pi = 6.783$) at $M = 0.9$ are $\beta = 0.662$ and $k_{\xi,\mp\infty} = \ell_{\xi,\mp\infty} = 5.580$, respectively.

In numerical calculations of the unsteady flow through a cascade, propagating acoustic disturbances and those which attenuate gradually with increasing distance from the blade row must be accurately represented. Thus for our example configuration, with

$M = 0.9$, acoustic waves with $k_\eta = 6.783$ and $k_\xi = 5.580$ must be resolved accurately. In this case, the computational mesh requirements are not stringent, but they can become so if either the Mach number or the excitation frequency is increased. In particular, in the foregoing example if $M = 0.95$ and $\sigma = 0$ deg, propagating ($\bar{\beta} = 0$) acoustic response disturbances with $k_{\eta,0} = 0$, $k_{\eta,1} = 6.28$ and $k_{\eta,2} = 13.57$ occur. The axial wave numbers of these propagating disturbances in the far upstream region, $k_{\xi,-\infty}$, are 2.89, 10.43 and 13.76, respectively. Consequently, small mesh spacings are required to capture the $n = 1$ and $n = 2$ acoustic response waves.

5.2.2 Supersonic Flow

Resonance curves for supersonic free-stream flows with subsonic axial velocity component are shown in figure 7. As $M \cos \Omega \rightarrow 1$ from below, both $\ell_\eta^{(+)}$ and $\ell_\eta^{(-)}$ approach the value $-M/(M^2 - 1)^{1/2}$. The locus of such points is shown as a dashed curve in figure 7. If $M \cos \Omega > 1$, the axial velocity is supersonic, resonance does not occur and acoustic response disturbances propagate only in the downstream axial direction. For supersonic flows with subsonic axial velocity component, the resonant condition $\ell_\eta = \ell_\eta^{(+)}$ varies substantially with Mach number, particularly at low supersonic Mach numbers. Indeed, $\ell_\eta^{(+)} \rightarrow -\infty$ as $M \rightarrow 1$ from above but, as in subsonic flow, $\ell_\eta^{(-)} \rightarrow -(2 \sin \Omega)^{-1}$. The extent of the superresonant region, i.e., $(\ell_\eta^{(+)}, \ell_\eta^{(-)})$, decreases with increasing Mach number and increases with increasing flow angle.

As a specific example, consider the case $\omega = 1$, $G = 1$, $V = 1$ and $\Omega = 60$ deg. The calculations leading to the curve for $\Omega = 60$ deg indicate that for a free-stream Mach number of 1.6 and interblade phase angles in the range $[-\pi, \pi]$ all acoustic response disturbances persist in the far field and carry energy away from the blade row if $\sigma < -2.037$ or $\sigma > -0.806$, but one such wave will attenuate with increasing distance from the blade row (the $n = 0$ wave) if $-2.037 < \sigma < -0.806$. For a Mach number of 1.4 the corresponding ranges are $\sigma < -2.810$, $\sigma > -0.727$ and $-2.810 < \sigma < -0.727$. Finally, for a Mach number of 1.2 the $n = 0$ acoustic response disturbance will be of decaying type if $-\pi \leq \sigma < -0.652$, the $n = -1$ disturbance will be of decaying type if $1.267 < \sigma \leq \pi$, but all disturbances are of propagating type if $-0.652 < \sigma < 1.267$. As the Mach number is reduced further, additional acoustic disturbances will be of decaying type.

Axial wave numbers and attenuation constants of the far-field acoustic response disturbances for Mach numbers of 1.1, 1.2, 1.3, 1.4 and 1.5 and a flow angle of 60 deg are shown in figure 8, and those for a Mach number of 1.3 and flow angles of 45 deg, 60 deg and 75 deg, in figure 9. Acoustic response disturbances at subresonant tangential wave numbers, i.e., $\ell_\eta \epsilon (-\infty, \ell_\eta^{(+)})$ or $\ell_\eta \epsilon (\ell_\eta^{(-)}, \infty)$, persist and carry energy away from the blade row. Thus acoustic response disturbances of high wave-number magnitude persist in the far field and, as such, they can impose serious limitations on the numerical field methods developed for predicting unsteady flows through cascades operating at supersonic inlet and/or exit conditions.

5.3 The Potential Response to Vortical Disturbances

The axial and tangential wave numbers of the potential response in the far downstream region caused by continuous rotational velocity fluctuations can also have high wave-number content (see (4.4)), but as indicated in (4.22), the amplitude of such potential disturbances varies inversely with wave-number magnitude. The potential response to shed (wake) vorticity has a wave-number vector of $-\omega V_{\infty}^{-1} \vec{e}_T$; hence, axial and tangential wave numbers of $k_{\xi} = -\omega V_{\infty}^{-1} \cos \Omega_{\infty}$ and $k_{\eta} = -\omega V_{\infty}^{-1} \sin \Omega_{\infty}$. The magnitude of this response fluctuation depends upon the discontinuities $[\phi]_{Ref}$ and $[\bar{v}^R]_{Ref}$ at the reference wake location (ξ_+, η_+) . The potential response due to this vorticity has a rather complicated behavior in the cascade circumferential direction that depends on the blade spacing, the downstream free-stream velocity and the temporal frequency and interblade phase angle of the unsteady excitation. For example, the function $\phi^R(\xi_+, \eta)/[\phi]_{Ref}$ is plotted vs. $\eta - \eta_+$ in figure 10 for a cascade with $G = 1$, operating in a downstream free stream with $V_{\infty} = 1$ and $\Omega_{\infty} = 45$ deg and subjected to non-vortical excitations, e.g., blade motions or incident acoustic waves, at $\sigma = 0$ deg and at various frequencies.

At the temporal frequencies of interest for practical applications, the potential distribution $\phi^R(\xi_+, \eta)$ in the cascade circumferential direction does not usually impose stringent requirements on the spacing of mesh lines parallel to the mean flow direction. However for certain parametric combinations, it can become necessary to pack such lines near the mean wake locations to resolve the potential fluctuation caused by wake vorticity.

6. NUMERICAL EXAMPLES: SUBSONIC FLOW

Our purposes in this section are to demonstrate the results that can be achieved by matching finite-difference near-field and analytic far-field solutions for the linearized unsteady potential and to illustrate important effects associated with the unsteady flow behavior in the far field on the aerodynamic response at a moving blade surface. We will restrict our consideration to two simple subsonic cascade configurations—a flat-plate cascade and a cascade of 5% thick flat-bottomed double-circular-arc (DCA) airfoils. In each case the cascade stagger angle Θ is 45 deg, the blade spacing G is unity and the inlet free-stream Mach number is 0.8. Also, the blades undergo pitching oscillations about midchord, i.e., $\vec{r} = \vec{\alpha} \times \vec{R}_p$ (see (2.1)), where $\vec{R}_p = \vec{X} - 0.5\vec{e}_x$. Such two dimensional blade motions model torsional vibrations of actual rotor blades.

Theoretical results will be presented for the complex amplitudes of the first harmonic unsteady aerodynamic moments,

$$m = \oint_B p_B \vec{R}_p \cdot d\vec{r}, \quad (6.1)$$

and pressure difference distributions,

$$\Delta p(x) = p_B(x, y_-) - p_B(x, y_+), \quad (6.2)$$

acting on the reference blade of each cascade. Here p_B is the complex amplitude of the first-harmonic pressure acting at the moving reference blade surface, the subscripts refer to the upper (+) and lower (−) surfaces of the blade and the integration is taken over the mean blade surface (B). Results will also be presented for the velocity potential distribution along the stagnation streamline that coincides with the upper surface of the reference blade.

We consider pitching (torsional) motions with $\alpha = 1$ at four different frequencies, $\omega = 0.5, 1.0, 1.5$, and 2.0 , and at interblade phase angles lying in the range $[-\pi, \pi]$. Since α is taken to be a real quantity, the real and imaginary components of a reference blade complex response parameter represent components that are in- and out-of-phase, respectively, with the reference blade displacement. The stability of a torsional blade motion depends upon the sign of the out-of-phase moment. If $Im\{\alpha\} = 0$ and $Im\{m\} > 0$, the airstream supplies energy to the blade motion and that motion is unstable according to linearized theory.

The steady flows through the flat plate and DCA cascades are assumed to satisfy a zero-load or Kutta condition, i.e.,

$$\vec{V} \cdot d\vec{r}|_{B_-} = -\vec{V} \cdot d\vec{r}|_{B_+} \quad (6.3)$$

at the leading and trailing edges of each blade. Therefore the inlet free-stream Mach number is the only far-field quantity needed to completely specify the mean potential

flow through the cascade. In particular, the steady flow through the example flat-plate cascade is simply a uniform stream with $M = 0.8$ and $\Omega = 45$ deg. For the DCA cascade operating at $M_{\infty} = 0.8$ the (calculated) inlet flow angle, exit Mach number and exit flow angle are 49.4 deg, 0.62 and 43 deg, respectively. This flow is entirely subsonic with a maximum Mach number of 0.941 occurring at a point on the suction surface which is 36.5% of blade chord downstream from the leading edge. The blade surface Mach number distribution is shown in figure 3 of Verdon & Caspar (1984). The wave-number behavior of the far-field acoustic response for the two example cascades is shown in figure 11.

Although linearized unsteady flow solutions for the example flat-plate cascade can be determined using semi-analytic surface-integral methods (e.g., see Smith 1971), the results presented herein for both the flat-plate and DCA cascades have been determined using the finite-difference numerical model described in Verdon & Caspar (1982, 1984). Those determined for the flat-plate cascade are in very good agreement with Smith's solutions. The finite-difference calculations were performed on a mesh composed of axial lines ($\xi = \text{constant}$) which are parallel to the blade row and tangential curves which are percentile averages of the upper and lower boundaries of the extended blade-passage solution domain. This mesh extended one axial chord upstream and downstream from the blade row (i.e., $-1 \leq \xi / \cos \Theta \leq 2$). For the most part uniform mesh spacings were used with $\Delta \xi = 0.03 \cos \Theta$ and $\Delta \eta = 3\%$ of the distance between the upper and lower boundaries, but mesh lines were concentrated near blade edges and near the upper and lower boundaries (i.e., the blades and their wakes) of the solution domain. The uniform spacings given above were selected so that the unsteady flows at the highest frequency considered, $\omega = 2.0$, could be resolved accurately over the entire interblade phase angle range $[-\pi, \pi]$.

6.1 Flat-Plate Cascade

Unsteady response predictions for the flat plate cascade operating in a uniform stream with $M = 0.8$ and $\Omega = 45$ deg are shown in figures 12 through 15. The resonant circumferential wave numbers in both the far upstream and far downstream regions for this configuration are $k_{\eta}^{(-)} = -0.575\omega$ and $k_{\eta}^{(+)} = 3.09\omega$. Acoustic response disturbances at circumferential wave numbers, $k_{\eta,n}$, lying between these values persist in both far-field regions and carry energy away from the blade row. Disturbances for which $k_{\eta,n} < k_{\eta}^{(-)}$ or $k_{\eta,n} > k_{\eta}^{(+)}$ attenuate with increasing distance from the blade row.

Unsteady moments due to torsional vibrations about midchord at $\omega = 0.5, 1.0, 1.5$ and 2.0 are shown in figure 12. The arrows above each curve indicate the resonant values of σ i.e., $\sigma^{(\mp)} = k_{\eta}^{(\mp)} / G - 2n\pi$ where $n = 0$ for $|k_{\eta}^{(\mp)} / G| \leq \pi$, $n = 1$ for $\pi < k_{\eta}^{(\mp)} / G < 3\pi$, etc., and therefore the boundaries between the different types of unsteady excitation. Note the abrupt changes in the unsteady moment that occur near resonance and, more importantly, the different character of the moment response in the different regions of unsteady excitation. For $\omega = 0.5$ and $\omega = 1.0$ the blade motions

are superresonant (1,1) with the $n = 0$ acoustic response disturbance persisting far upstream and far downstream of the blade row for values of σ lying between the two resonant values. The blade motions at $\omega = 0.5$ and $\omega = 1.0$ are subresonant for $\sigma \epsilon [-\pi, \sigma^{(-)}]$ and $\sigma \epsilon (\sigma^{(+)}, \pi]$. At $\omega = 1.5$ the blade motions are superresonant (1,1) for $\sigma \epsilon [-\pi, \sigma^{(+)})$ and $\sigma \epsilon (\sigma^{(-)}, \pi]$, and subresonant for $\sigma \epsilon (\sigma^{(+)}, \sigma^{(-)})$. In the first case the $n = 1$ acoustic response disturbance is of propagating type and in the second the $n = 0$ disturbance is of propagating type. The flat-plate blade motions at $\omega = 2$ are superresonant at all interblade phase angles. These motions are superresonant (1,1) for $\sigma \epsilon (-\pi, \sigma^{(-)})$ and $\sigma \epsilon (\sigma^{(+)}, \pi)$ and superresonant (2,2) for $\sigma \epsilon (\sigma^{(-)}, \sigma^{(+)})$. In the first case the $n = 1$ acoustic response disturbance is of propagating type, in the second the $n = 0$ disturbance is of propagating type and in the third both the $n = 0$ and the $n = 1$ acoustic response disturbances are of propagating type. The foregoing information is summarized in Table 1.

Table 1. Unsteady far-field behavior for the flat-plate cascade

Excitation frequency and resonant phase angles	Interblade phase angle range	Type of blade motion	Propagating Waves upstream/downstream
$\omega = 0.5$	$[-\pi, \sigma^{(-)})$	subresonant	none/none
$\sigma^{(-)} = -0.288$	$(\sigma^{(-)}, \sigma^{(+)})$	superresonant(1,1)	$n=0/n=0$
$\sigma^{(+)} = 1.545$	$(\sigma^{(+)}, \pi]$	subresonant	none/none
$\omega = 1.0$	$[-\pi, \sigma^{(-)})$	subresonant	none/none
$\sigma^{(-)} = -0.575$	$(\sigma^{(-)}, \sigma^{(+)})$	superresonant	$n=0/n=0$
$\sigma^{(+)} = 3.090$	$(\sigma^{(+)}, \pi]$	subresonant	none/none
$\omega = 1.5$	$[-\pi, \sigma^{(+)})$	superresonant(1,1)	$n=1/n=1$
$\sigma^{(-)} = -0.853$	$(\sigma^{(+)}, \sigma^{(-)})$	subresonant	none/none
$\sigma^{(+)} = -1.647$	$(\sigma^{(-)}, \pi]$	superresonant(1,1)	$n=0/n=0$
$\omega = 2.0$	$[-\pi, \sigma^{(-)})$	superresonant(1,1)	$n=1/n=1$
$\sigma^{(-)} = -1.150$	$(\sigma^{(-)}, \sigma^{(+)})$	superresonant(2,2)	$n=0,1/n=0,1$
$\sigma^{(+)} = -0.103$	$(\sigma^{(+)}, \pi]$	superresonant(1,1)	$n=0/n=0$

Unsteady pressure difference distributions for the example flat-plate cascade with blades vibrating at $\omega = 0.5, 1.0, 1.5$ and 2.0 are shown in figure 13 for $\sigma = -1$ and in figure 14 for $\sigma = 2$. The blade motions at $\sigma = -1$ are subresonant at the three lower frequencies and superresonant (2,2) at $\omega = 2$. In the latter case the propagating acoustic response waves have wave numbers (k_ξ, k_n) of $(1.778, -1)$ and $(5.931, 5.283)$ in the far upstream region and $(-0.577, -1)$ and $(1.738, 5.283)$ in the far downstream region. The blade motion at $\sigma = 2$ and $\omega = 0.5$ is subresonant. The motions at $\sigma = 2$ and $\omega = 1.0, 1.5$, and 2.0 are superresonant (1,1) with wave numbers of $(3.085,$

2), (4.362, 2) and (5.474, 2), respectively, in the far upstream region and (0.129, 2), (-0.483, 2) and (-0.930, 2), respectively, in the far downstream region. The pressure difference curves for $\sigma = -1$ differ substantially for the four frequencies considered. One reason for this is that the motions at $\sigma = -1$ occur close to the resonance condition $\sigma^{(-)} = -0.575\omega$, particularly those at the two higher frequencies. In contrast, the blade motions at $\sigma = 2$ lie well within the subresonant region for $\omega = 0.5$ and well within the superresonant region for $\omega = 1.0, 1.5$ and 2.0 . Thus, although the magnitudes of the unsteady pressure differences (and the unsteady moments) tend to be much greater for the motion at $\omega = 0.5$ than for those at $\omega = 1.0, 1.5$ and 2.0 , the pressure difference curves for $\sigma = 2$ show a consistent trend with increasing frequency. Note that at both phase angles, $\sigma = -1$ and $\sigma = 2$, the pressure difference curves show higher wave-number content with increasing temporal frequency.

Unsteady potential distributions on the first tangential line of the computational mesh used for the flat-plate calculations (i.e., on $y = 0^+$) are shown in figure 15 for blade motions occurring at $\sigma = -1$ and $\omega = 1$, $\sigma = 2$ and $\omega = 0.5$, $\sigma = 2$ and $\omega = 1$ and at $\sigma = -1$ and $\omega = 2$. The results for $-1 < \xi/\cos\Theta < 2$ have been determined from the finite difference calculation, those for $\xi/\cos\Theta < -1$ and $\xi/\cos\Theta > 2$, from the analytic far-field solutions. The two solutions were matched at $\xi/\cos\Theta = -1$ and $\xi/\cos\Theta = 2$. The potential in the far upstream region, $\phi = \phi^P$, is due solely to the acoustic response to the blade motion, while that in the far downstream region, $\phi = \phi^P + \phi^R$, depends also upon the vorticity shed from the blades. The potential fluctuation ϕ^R has a wave number in the streamwise (in this case the $x-$) direction of $-\omega$. The blade motions at $\sigma = -1$ and $\omega = 1$ and at $\sigma = 2$ and $\omega = 0.5$ are subresonant, so $\phi^P \rightarrow 0$ as $|\xi| \rightarrow \infty$. In both cases the potential fluctuation in the far downstream region is due essentially to wake vorticity. However, as seen from the potential distribution in the far upstream region, the $n = 0$ acoustic response wave for the blade motion at $\sigma = 2$ and $\omega = 0.5$ attenuates only gradually with increasing distance from the blade row. The acoustic response to the superresonant (1,1) blade motion at $\sigma = 2$ and $\omega = 1$ has a streamwise wave number of $k_x = 3.596$ in the far upstream region and $k_x = 1.505$ in the far downstream region. The potential fluctuation due to the acoustic response in the far downstream region occurs at a much smaller amplitude than the fluctuation due to wake vorticity. Finally, the acoustic response to the superresonant (2,2) blade motion at $\sigma = -1$ and $\omega = 2$ has streamwise wave numbers of 0.550 and 7.92 in the far upstream region and -1.115 and 4.965 in the far downstream region. The acoustic disturbances at the higher wave numbers occur at much smaller amplitude than those at the lower wave numbers.

6.2 The DCA Cascade

Unsteady response predictions for the example DCA cascade are presented in figures 16 through 19. Since the inlet ($M_{-\infty} = 0.8, \Omega_{-\infty} = 49.4$ deg) and exit ($M_\infty = 0.62, \Omega_\infty = 43$ deg) free-stream conditions differ for this configuration, the acoustic

response characteristics in the far upstream and far downstream regions also differ. In particular, the resonant circumferential wave numbers are $k_{\eta,-\infty}^{(-)} = -0.547\omega$ and $k_{\eta,-\infty}^{(+)} = 3.247\omega$ in the far upstream region and $k_{\eta,\infty}^{(-)} = -0.595\omega$ and $k_{\eta,\infty}^{(+)} = 1.669\omega$ in the far downstream region. Acoustic response disturbances occurring at circumferential wave numbers, $k_{\eta,n}$, lying between $k_{\eta,-\infty}^{(-)}$ and $k_{\eta,-\infty}^{(+)}$ persist in the far upstream region, and those occurring at circumferential wave numbers lying between $k_{\eta,\infty}^{(-)}$ and $k_{\eta,\infty}^{(+)}$ persist in the far downstream region.

The unsteady moments over the interblade phase angle range $[-\pi, \pi]$ are shown in figure 16 for torsional blade vibrations at $\omega = 0.5, 1.0, 1.5$ and 2.0 . Again the arrows (now four) above each curve indicate the resonant interblade phase angles. Because of the different acoustic environments in the two far-field regions, it is a more difficult task to classify the DCA blade motions. For example, consider the blade motions at $\omega = 1$. Those occurring in the range $(\sigma_{-\infty}^{(+)}, \sigma_{\infty}^{(-)})$ are subresonant, and therefore the acoustic response to the blade motion attenuates with increasing distance from the blade row. Blade motions at the other non-resonant interblade phase angles are superresonant. In particular, these motions are superresonant $(1,0)$, $(0,1)$, $(1,1)$ and $(1,0)$ for interblade phase angles lying in the ranges $[-\pi, \sigma_{-\infty}^{(+)})$, $(\sigma_{\infty}^{(-)}, \sigma_{-\infty}^{(-)})$, $(\sigma_{-\infty}^{(-)}, \sigma_{\infty}^{(+)})$ and $(\sigma_{\infty}^{(+)}, \pi]$, respectively. In the first case the $n = 1$ acoustic response disturbance persists in the far upstream region; in the second, the $n = 0$ disturbance persists far downstream; in the third, the $n = 0$ disturbances persist in both far-field regions; and, finally, in the fourth, the $n = 0$ disturbance persists far upstream. This information is summarized in Table 2 below along with the corresponding results for the DCA blade motions at $\omega = 0.5, 1.5$ and 2.0 . There are significant differences between the unsteady moment responses to the flat-plate and DCA blade motions. These differences can be attributed to the effects of mean flow variations near the surfaces of the DCA blades and to the different far-field acoustic response environments seen by the two cascades.

Unsteady pressure difference distributions for the DCA cascade are shown in figures 17 and 18 for torsional blade motions at $\sigma = -1$ and $\sigma = 2$, respectively. The motions at $\sigma = -1$ are subresonant for $\omega = 0.5, 1.0$ and 1.5 and superresonant $(2,1)$ for $\omega = 2.0$. In the superresonant case the wave numbers (k_ξ, k_η) of the propagating acoustic disturbances are $(1.403, -1)$ and $(5.720, 5.283)$ in the far upstream region and $(-0.245, -1)$ in the far downstream region. For $\sigma = 2$ the blade motion at $\omega = 0.5$ is subresonant and those at $\omega = 1.0, 1.5$ and 2.0 are superresonant. The superresonant $(1,0)$ motion at $\sigma = 2$ and $\omega = 1.0$ produces an upstream propagating acoustic response disturbance at $(k_\xi, k_\eta) = (2.906, 2)$. For the superresonant $(1,1)$ motion at $\sigma = 2$ and $\omega = 1.5$ the wave numbers of the acoustic response are $(4.067, 2)$ far upstream and $(-0.039, 2)$ far downstream. Finally, for the superresonant $(1,1)$ blade motion at $\sigma = 2$ and $\omega = 2$ the propagating acoustic disturbances occur at $(5.080, 2)$ far upstream and $(-0.665, 2)$ far downstream.

Table 2. Unsteady far-field behavior for the DCA cascade

Excitation frequency and resonant phase angles	Interblade phase angle range	Type of blade motion	Propagating Waves upstream/downstream
$\omega = 0.5$	$[-\pi, \sigma_{\infty}^{(-)})$	subresonant	none/none
$\sigma_{-\infty}^{(-)} = -0.274$	$(\sigma_{\infty}^{(-)}, \sigma_{-\infty}^{(-)})$	superresonant(0,1)	none/n=0
$\sigma_{-\infty}^{(+)} = 1.624$	$(\sigma_{-\infty}^{(-)}, \sigma_{\infty}^{(+)})$	superresonant(1,1)	n=0/n=0
$\sigma_{\infty}^{(-)} = -0.297$	$(\sigma_{\infty}^{(+)}, \sigma_{-\infty}^{(+)})$	superresonant(1,0)	n=0/n=0
$\sigma_{\infty}^{(+)} = 0.834$	$(\sigma_{-\infty}^{(+)}, \pi)$	subresonant	none/none
$\omega = 1$	$[-\pi, \sigma_{-\infty}^{(+)})$	superresonant(1,0)	n=1/none
$\sigma_{-\infty}^{(-)} = -0.547$	$(\sigma_{-\infty}^{(+)}, \sigma_{\infty}^{(-)})$	subresonant	none/none
$\sigma_{-\infty}^{(+)} = -3.037$	$(\sigma_{\infty}^{(-)}, \sigma_{-\infty}^{(-)})$	superresonant(0,1)	none/n=0
$\sigma_{\infty}^{(-)} = -0.595$	$(\sigma_{-\infty}^{(-)}, \sigma_{\infty}^{(+)})$	superresonant(1,1)	n=0/n=0
$\sigma_{\infty}^{(+)} = 1.669$	$(\sigma_{\infty}^{(+)}, \pi]$	superresonant(1,0)	n=0/none
$\omega = 1.5$	$[-\pi, \sigma_{-\infty}^{(+)})$	superresonant(1,0)	n=1/none
$\sigma_{-\infty}^{(-)} = -0.821$	$(\sigma_{-\infty}^{(+)}, \sigma_{\infty}^{(-)})$	subresonant	none/none
$\sigma_{-\infty}^{(+)} = -1.413$	$(\sigma_{\infty}^{(-)}, \sigma_{-\infty}^{(-)})$	superresonant(0,1)	none/n=0
$\sigma_{\infty}^{(-)} = -0.892$	$(\sigma_{-\infty}^{(-)}, \sigma_{\infty}^{(+)})$	superresonant(1,1)	n=0/n=0
$\sigma_{\infty}^{(+)} = 2.503$	$(\sigma_{\infty}^{(+)}, \pi]$	superresonant(1,0)	n=0/none
$\omega = 2$	$[-\pi, \sigma_{\infty}^{(+)})$	superresonant(1,1)	n=1/n=1
$\sigma_{-\infty}^{(-)} = -1.095$	$(\sigma_{\infty}^{(+)}, \sigma_{\infty}^{(-)})$	superresonant(1,0)	n=1/none
$\sigma_{-\infty}^{(+)} = 0.218$	$(\sigma_{\infty}^{(-)}, \sigma_{-\infty}^{(-)})$	superresonant(1,1)	n=1/n=0
$\sigma_{\infty}^{(-)} = -1.190$	$(\sigma_{-\infty}^{(-)}, \sigma_{-\infty}^{(+)})$	superresonant(2,1)	n=0,1/n=0
$\sigma_{\infty}^{(+)} = -2.947$	$(\sigma_{-\infty}^{(+)}, \pi]$	superresonant(1,1)	n=0/n=0

The pressure difference curves for the DCA and flat-plate blades vibrating at $\sigma = -1$ show similar behaviors for $\omega = 0.5$ and, except near the blade leading edge, $\omega = 1.0$. Here, the differences between the DCA and flat-plate results are due primarily to the nonuniform mean flow over the DCA blade surfaces. The responses to the DCA and flat-plate blade motions at $\sigma = -1$ differ considerably for $\omega = 1.5$ and $\omega = 2$. These motions occur near a resonance condition and, as we shall see more clearly below, the flat-plate and DCA blade motions produce very different acoustic responses in the far field. The pressure difference curves for the DCA and flat-plate blade motions at $\sigma = 2$ are quite similar for the subresonant blade motions at $\omega = 0.5$ but differ considerably for the superresonant motions at $\omega = 1.0, 1.5$ and 2.0 . Again, the differences can be attributed to the nonuniform mean flow over the surface of each DCA blade and to the different far downstream acoustic response environments seen by the two cascades. For

example, at $\sigma = 2$ and $\omega = 1$ an acoustic response fluctuation persists far downstream of the flat-plate cascade, but all such disturbances attenuate with increasing distance downstream of the DCA cascade.

Unsteady potential distributions on the lower boundary of the extended blade passage solution domain (i.e., the stagnation streamline that coincides with the upper surface of the reference blade) are shown in figure 19 for DCA blade motions at $\sigma = -1$ and $\omega = 1$, $\sigma = 2$ and $\omega = 0.5$, $\sigma = 2$ and $\omega = 1$ and for $\sigma = -1$ and $\omega = 1$. Again, the results for $-1 < \xi / \cos \Theta < 2$ have been determined from the finite-difference near-field solution and those for $\xi / \cos \Theta < -1$ and $\xi / \cos \Theta > 2$ from the analytic far-field solutions. The far downstream potential for the first three of these motions is essentially due to wake vorticity and therefore has a wave number of $-\omega V_\infty^{-1} = -1.26\omega$ in the streamwise direction. The DCA blade motions at $\sigma = -1$ and $\omega = 1$ and at $\sigma = 2$ and $\omega = 0.5$ are subresonant, and the far-field behavior associated with these motions is similar to that observed for the flat plate cascade. The far upstream acoustic response to the superresonant (1,0) blade motion at $\sigma = 2$ and $\omega = 1$ occurs at a streamwise wave number of 3.409 and at a much larger amplitude than the upstream propagating wave generated by the corresponding flat-plate blade motion. Finally, the acoustic response to the superresonant (2,1) motion at $\sigma = -1$ and $\omega = 2$ has streamwise wave numbers of 0.154 and 7.734 in the far upstream region and -0.861 in the far downstream region. As can be seen from the results in figures 15 and 19, the far-field response associated with this motion differs considerably from that produced by the flat-plate blade vibrations at $\sigma = -1$ and $\omega = 2$.

7. CONCLUDING REMARKS

Analytic solutions for the unsteady velocity potential response far upstream and far downstream of an isolated two-dimensional cascade and for the rotational velocity response far downstream have been provided. Fourier series representations account for the continuous response fluctuations associated with acoustic disturbances, which either attenuate with increasing axial distance from the blade row or persist and carry energy away from or parallel to the blade row, and the rotational velocity disturbances which are convected through the blade row. Closed form expressions account for the discontinuous response fluctuations associated with the concentrated vorticity convected along blade wakes. The complete far-field solution provides the upstream and downstream information needed for formulating the boundary-value problem that describes the linearized unsteady perturbation of an irrotational and isentropic mean flow through a cascade. In addition, this complete solution can be easily implemented into the numerical analyses and computer codes developed to predict the aerodynamic response of the blading to prescribed small-amplitude unsteady excitations, i.e., blade motions and incident entropic, vortical and acoustic disturbances.

Special cases of the far-field solutions presented herein have been used for some time in unsteady aerodynamic analyses intended for blade flutter prediction in which prescribed blade motions are the only source of unsteady excitation. However, the solutions provided in this report apply more generally to forced vibration problems in which blade motions caused by incident external aerodynamic disturbances are also of concern. The Fourier series representation of the far-field acoustic response is particularly well-suited for cascades operating at subsonic inlet and exit Mach number since only a limited number of acoustic response disturbances can persist in the far field. However, as indicated by our numerical results for flat-plate and DCA cascades, there is a complex and interesting variety of far-field response phenomena even for subsonic flows. This phenomena must be represented accurately in order to predict correctly the aerodynamic response at a vibrating blade surface. At high subsonic inlet and exit Mach numbers and at the high excitation frequencies typical of forced blade vibrations, stringent mesh spacing requirements must be imposed in numerical calculations of unsteady flows through blade rows. For a supersonic free-stream flow with subsonic axial velocity component an infinite number of acoustic response disturbances will persist in the far field. Since only a finite number of these disturbances can be modeled on a computational grid, the usefulness of the Fourier series representation of the far-field acoustic response for such flows must still be carefully evaluated.

REFERENCES

- Adamczyk, J. J. 1978 Analysis of supersonic stall bending flutter in axial-flow compressors by actuator disk theory. *NASA TP-1345*.
- Ashley, H. & Landahl, M. 1965 *Aerodynamics of Wings and Bodies*. Addison-Wesley.
- Atassi, H. M. 1987 Unsteady vortical disturbances around bodies. In *Proceedings of the 10th U. S. National Congress of Applied Mechanics*, ASME New York.
- Atassi, H. & Akai, T. J. 1980 Aerodynamic and aeroelastic characteristics of oscillating loaded cascades at low Mach number, I. pressure distribution, forces and moments. *Trans. ASME A: Journal of Engineering for Power* **102**, 344.
- Bendiksen, O. O. 1986 Asymptotic solutions for unsteady flows in cascades. *Quarterly of Applied Mathematics* **XLIV**, 493.
- Caruthers, J. E. 1981 Aerodynamic analysis of cascade airfoils in unsteady rotational flow. In *Proceedings 2nd International Symposium on Aeroelasticity in Turbomachines* (ed. P. Suter), pp. 31–64. Juris-Verlag, Zurich.
- Fransson, T. H. & Pandolfi, M. 1986 Numerical investigation of unsteady subsonic compressible flows through an oscillating cascade. *ASME 31st International Gas Turbine Conference; Paper 86-GT-304*.
- Giles, M. B. 1987 Calculations of unsteady wake/rotor interactions. *AIAA 25th Aerospace Sciences Meeting; Paper 87-006*.
- Goldstein, M. E. 1978 Unsteady vortical and entropic distortions of potential flows round arbitrary obstacles. *Journal of Fluid Mechanics* **89**, 433.
- Goldstein, M. E. 1979 Turbulence generated by the interaction of entropy fluctuations with non-uniform mean flows. *Journal of Fluid Mechanics* **93**, 209.
- Landahl, M. 1961 *Unsteady Transonic Flow*. Pergamon Press.
- Miles, J. W. 1959 *The Potential Theory of Unsteady Supersonic Flow*. Cambridge University Press.
- Ni, R. H. 1979 A rational analysis of periodic flow perturbation in supersonic two-dimensional cascade. *Trans. ASME A: Journal of Engineering for Power* **101**, 431.
- Rai, M. M. 1985 Navier-Stokes simulations of rotor-stator interaction using patched and overlaid grids. *AIAA 7th Computational Fluid Dynamics Conference; Paper 85-1519*.
- Samoilovich, G. S. 1967 Resonance phenomena in sub- and supersonic flow through an aerodynamic cascade. *Mekhanika Zhidkosti i Gaza* **2**, 143.

- Smith, S. N. 1971 Discrete frequency sound generation in axial flow turbomachines. *British Aeronautical Research Council, R&M* 3709.
- Usab, W. J., Jr. & Verdon, J. M. 1986 On the application of a linearized unsteady potential flow analysis to two-dimensional fan-tip cascades. *Trans. ASME: Journal of Turbomachinery* **108**, 59.
- Verdon, J. M. 1979 Further developments in the aerodynamic analysis of unsteady supersonic cascades—Part 1: The unsteady pressure field,—Part 2: Aerodynamic response predictions. *Trans. ASME A: Journal of Engineering for Power* **101**, 431.
- Verdon, J. M. 1987a Unsteady aerodynamics of blade rows. In *Proceedings of the Tenth U. S. National Congress of Applied Mechanics*, ASME. New York.
- Verdon, J. M. 1987b Linearized unsteady aerodynamic theory. In *AGARD Manual on Aeroelasticity in Axial-Flow Turbomachines* (eds. M. F. Platzer & F. O. Carta) I, Chapter 2.
- Verdon, J. M., Adamczyk, J. J. & Caspar, J. R. 1975 Subsonic flow past an oscillating cascade with steady blade loading—basic formulation. In *Proceedings of Symposium on Unsteady Aerodynamics* (ed. R. B. Kinney), II, pp. 827–851. Arizona.
- Verdon, J. M. & Caspar, J. R. 1982 Development of a linear unsteady aerodynamic analysis for finite-deflection subsonic cascades. *AIAA Journal* **20**, 1259.
- Verdon, J. M. & Caspar, J. R. 1984 A linearized unsteady aerodynamic analysis for transonic cascades. *Journal of Fluid Mechanics* **149**, 403.
- Whitehead, D. S. 1982 The calculation of steady and unsteady transonic flow in cascades. *Cambridge Univ. Engineering Department Report CUED/A-Turbo/TR* 118.
- Whitehead, D. S. 1987 Classical two-dimensional methods. In *AGARD Manual on Aeroelasticity in Axial-Flow Turbomachines* (eds. M. F. Platzer & F. O. Carta) I, Chapter 3.
- Whitehead, D. S. & Davies, M. R. D. 1983 An actuator disc analysis of unsteady supersonic cascade flow. *Journal of Sound and Vibration* **88**, 197.

LIST OF FIGURES

- Figure 1. Two-dimensional subsonic compressor cascade; $M_\infty < M_{-\infty} < 1$.
- Figure 2. Far-field acoustic response behavior for subsonic flow; the first number listed under each region refers to the inequality satisfied by $k_{\eta,n}$, the second to the expression used to determine χ_n .
- Figure 3. Far-field acoustic response behavior for supersonic flow; the first number listed under each region refers to the inequality satisfied by $k_{\eta,n}$, the second to the expression used to determine χ_n .
- Figure 4. Resonance conditions for an isolated blade row operating in a subsonic free stream.
- Figure 5. Effect of Mach number on the far-field acoustic response of an isolated blade row operating in a subsonic free stream; $\Omega = 45$ deg: (a) axial wave number vs. circumferential wave number; (b) attenuation constant vs. circumferential wave number.
- Figure 6. Effect of flow angle on the far-field acoustic response of an isolated blade row operating in a subsonic free stream; $M = 0.8$: (a) and (b) as in figure 5.
- Figure 7. Resonance conditions for an isolated blade row operating in a supersonic free stream.
- Figure 8. Effect of Mach number on the far-field acoustic response of an isolated blade row operating in a supersonic free stream; $\Omega = 60$ deg: (a) axial wave number vs. circumferential wave number; (b) attenuation constant vs. circumferential wave number.
- Figure 9. Effect of flow angle on the far-field acoustic response of an isolated blade row operating in a supersonic free stream; $M = 1.3$: (a) and (b) as in figure 8.
- Figure 10. The potential response to concentrated wake vorticity; $G = 1$, $V_\infty = 1$, $\Omega_\infty = 45$ deg, $\sigma = 0$.
- Figure 11. Axial vs. circumferential wave number of the far-field acoustic response associated with the example cascades; $G = 1$, $\Theta = 45$ deg: (a) flat-plate cascade; $M = 0.8$, $\Omega = 45$ deg; (b) DCA Cascade; $M_{-\infty} = 0.8$, $\Omega_{-\infty} = 49.4$ deg, $M_\infty = 0.62$, $\Omega_\infty = 43$ deg.
- Figure 12. Unsteady moment vs. interblade phase angle for torsional blade vibrations of the example flat-plate cascade: —— in-phase component (real part); —— out-of-phase component (imaginary part).
- Figure 13. Unsteady pressure difference distributions due to torsional blade vibrations

at $\sigma = -1$ for the example flat-plate cascade: (a) in-phase component; (b) out-of-phase component.

Figure 14. Unsteady pressure difference distributions due to torsional blade vibrations at $\sigma = 2$ for the example flat-plate cascade: (a) in-phase component; (b) out-of-phase component.

Figure 15. Unsteady potential distributions on $y = 0^+$ for torsional blade vibrations of the the example flat-plate cascade; numerical solution domain extends over $-1 \leq \xi / \cos \Theta \leq 2$: $--$ in-phase component; $-$ out-of-phase component.

Figure 16. Unsteady moment vs. interblade phase angle for torsional blade vibrations of the example DCA cascade: $--$ in-phase component (real part); $-$ out-of-phase component (imaginary part).

Figure 17. Unsteady pressure difference distributions due to torsional blade vibrations at $\sigma = -1$ for the example DCA cascade: (a) in-phase component; (b) out-of-phase component.

Figure 18. Unsteady pressure difference distributions due to torsional blade vibrations at $\sigma = 2$ for the example DCA cascade: (a) in-phase component; (b) out-of-phase component.

Figure 19. Unsteady potential distributions along the reference stagnation streamline for torsional blade vibrations of the the example DCA cascade; numerical solution domain extends over $-1 \leq \xi / \cos \Theta \leq 2$: $--$ in-phase component; $-$ out-of-phase component.

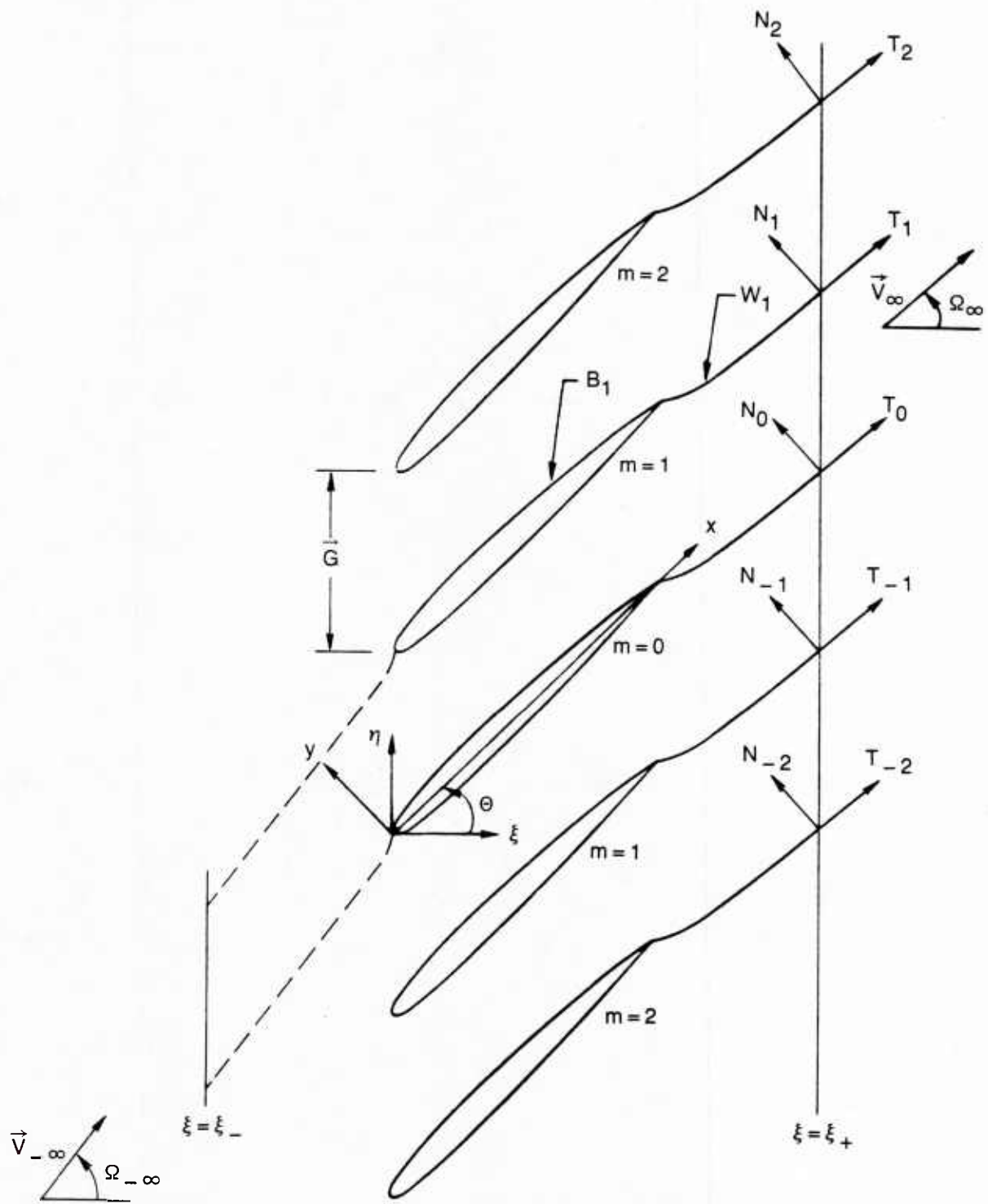


Figure 1. Two-dimensional subsonic compressor cascade; $M_\infty < M_{-\infty} < 1$.

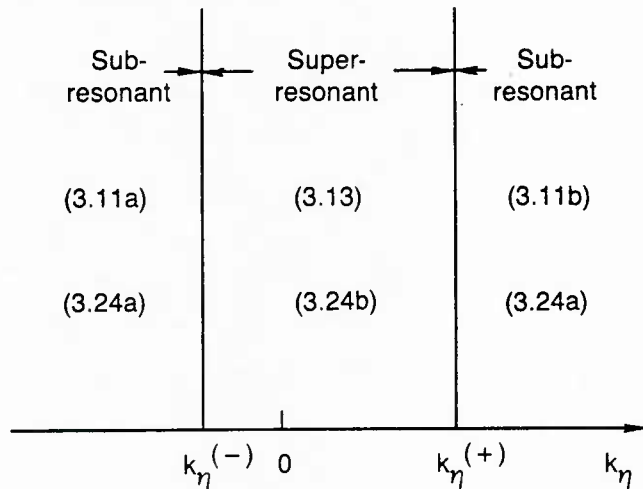
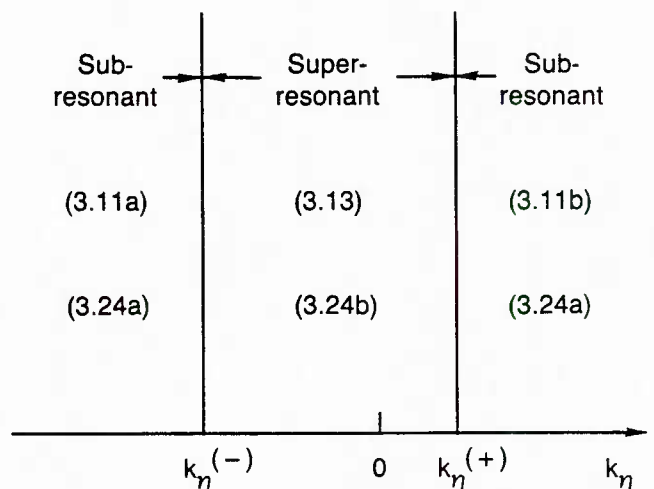
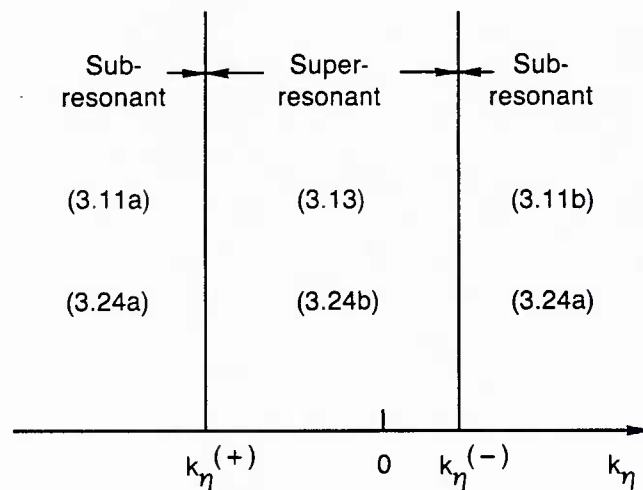
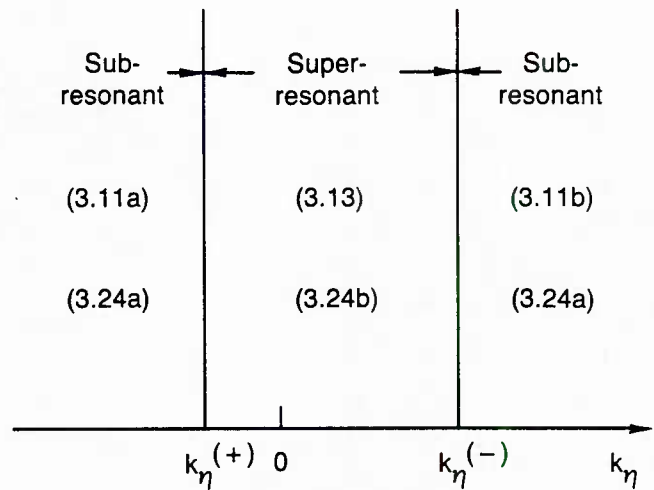
a) $\omega > 0, \Omega > 0$ b) $\omega > 0, \Omega < 0$ c) $\omega < 0, \Omega > 0$ d) $\omega < 0, \Omega < 0$ 

Figure 2. Far-field acoustic response behavior for subsonic flow; the first number listed under each region refers to the inequality satisfied by $k_{\eta,n}$, the second to the expression used to determine χ_n .

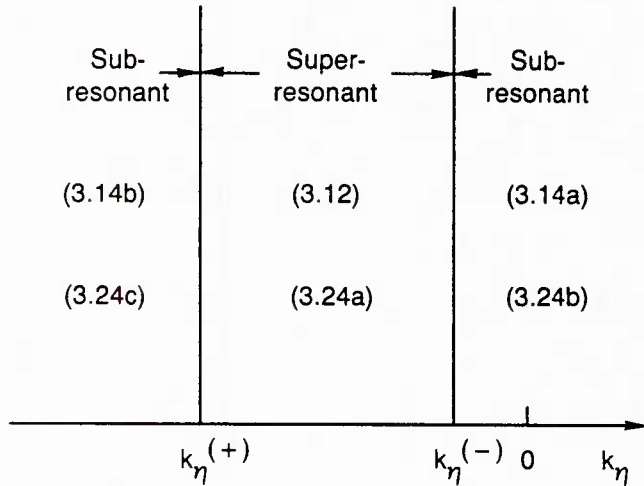
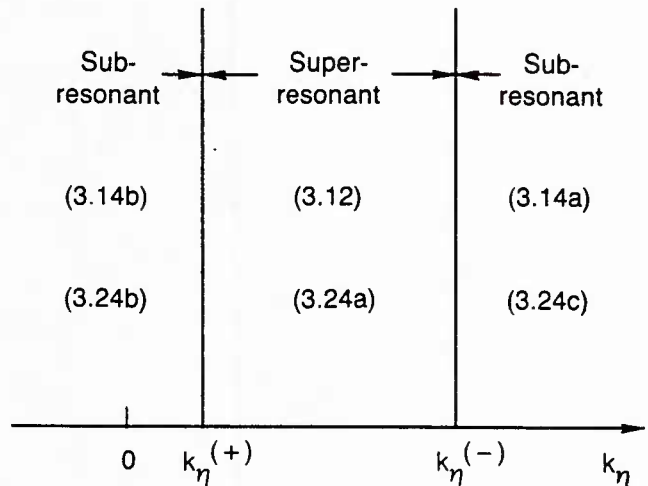
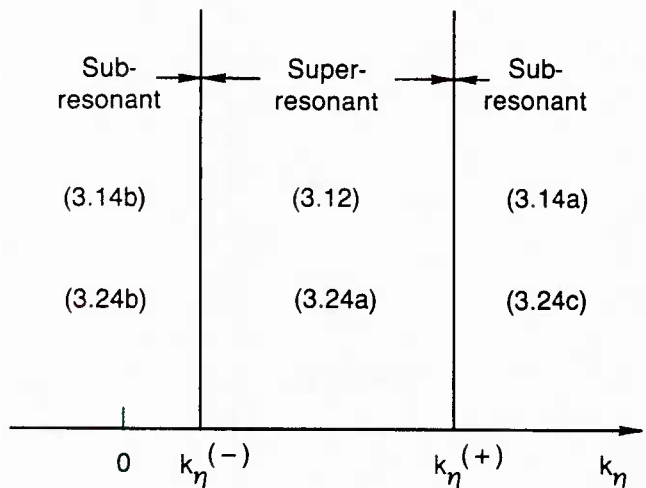
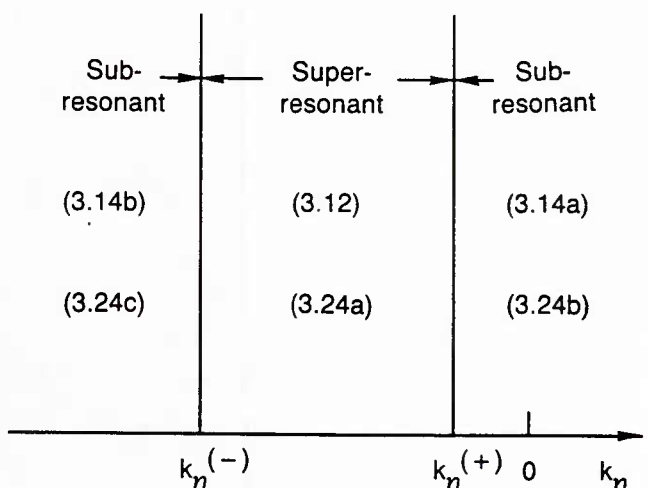
a) $\omega > 0, \Omega > 0$ b) $\omega > 0, \Omega < 0$ c) $\omega < 0, \Omega > 0$ d) $\omega < 0, \Omega < 0$ 

Figure 3. Far-field acoustic response behavior for supersonic flow; the first number listed under each region refers to the inequality satisfied by $k_{\eta,n}$, the second to the expression used to determine χ_n .

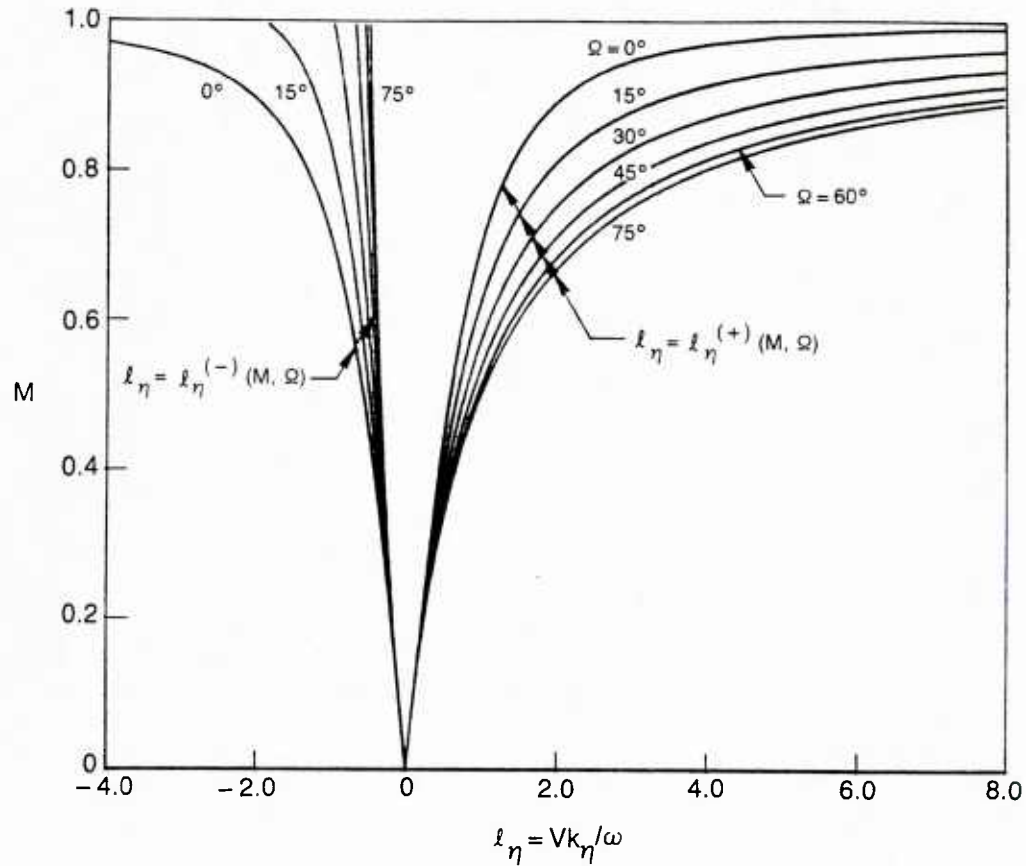


Figure 4. Resonance conditions for an isolated blade row operating in a subsonic free stream.

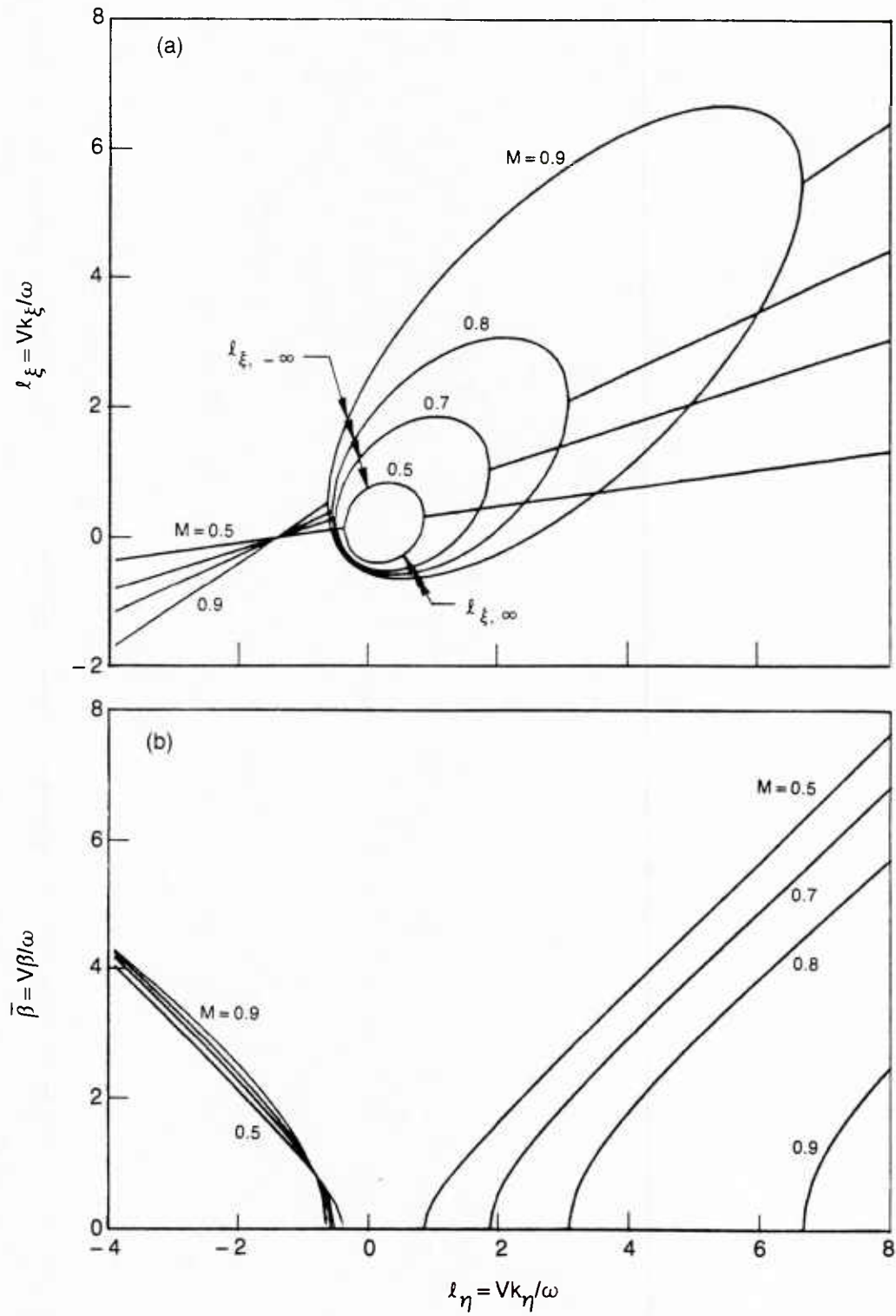


Figure 5. Effect of Mach number on the far-field acoustic response of an isolated blade row operating in a subsonic free stream; $\Omega = 45$ deg:
(a) axial wave number vs. circumferential wave number; (b) attenuation constant vs. circumferential wave number.

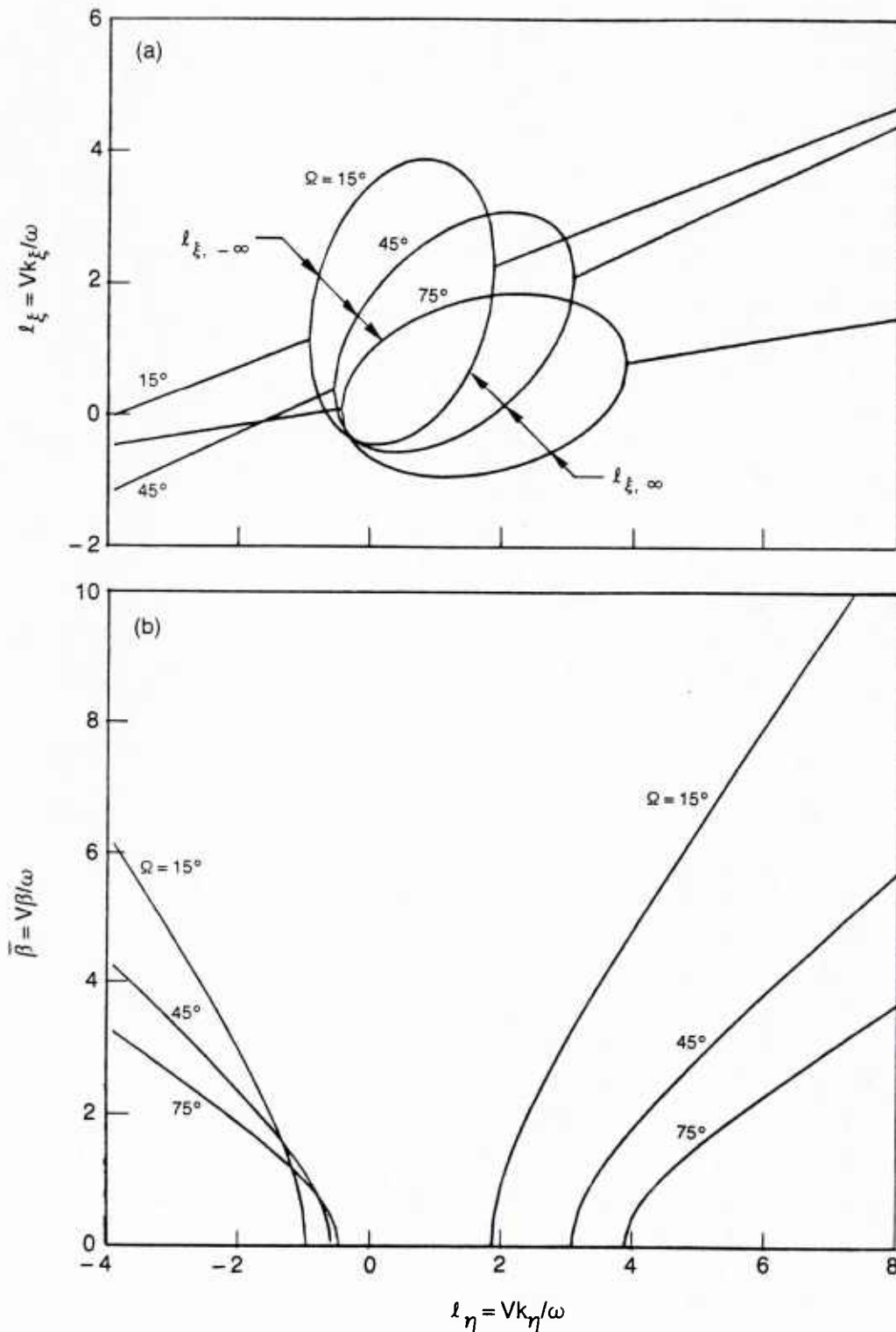


Figure 6. Effect of flow angle on the far-field acoustic response of an isolated blade row operating in a subsonic free stream; $M = 0.8$: (a) and (b) as in figure 5.

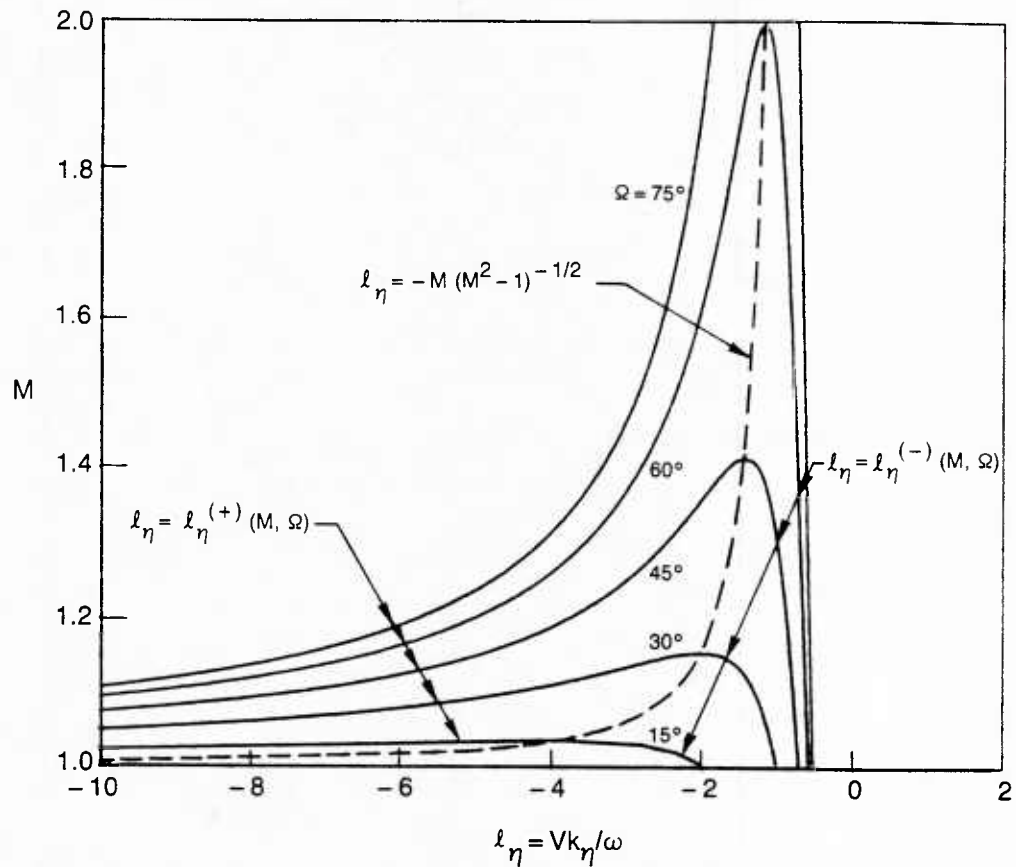


Figure 7. Resonance conditions for an isolated blade row operating in a supersonic free stream.

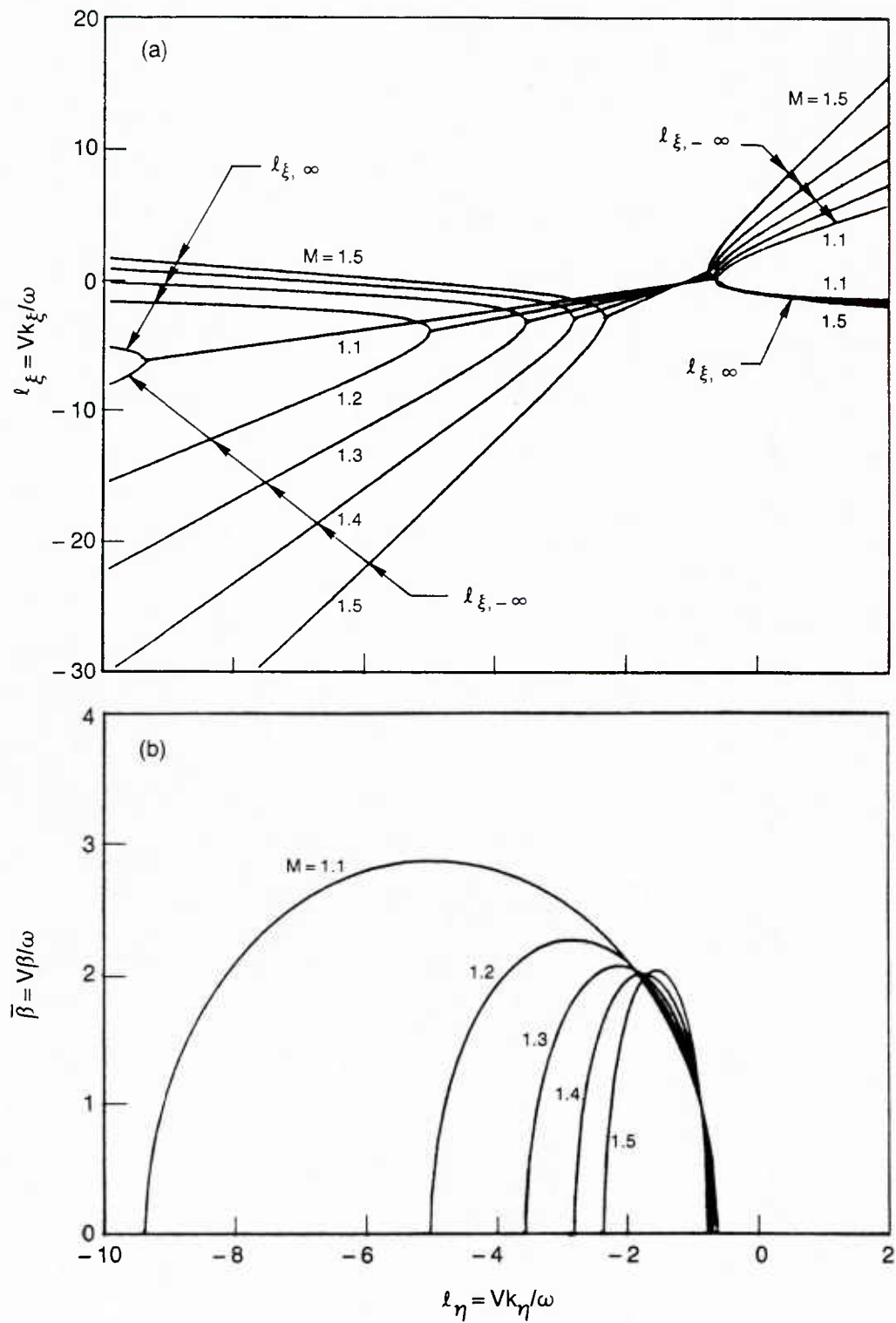


Figure 8. Effect of Mach number on the far-field acoustic response of an isolated blade row operating in a supersonic free stream; $\Omega = 60$ deg:
(a) axial wave number vs. circumferential wave number; **(b)** attenuation constant vs. circumferential wave number.

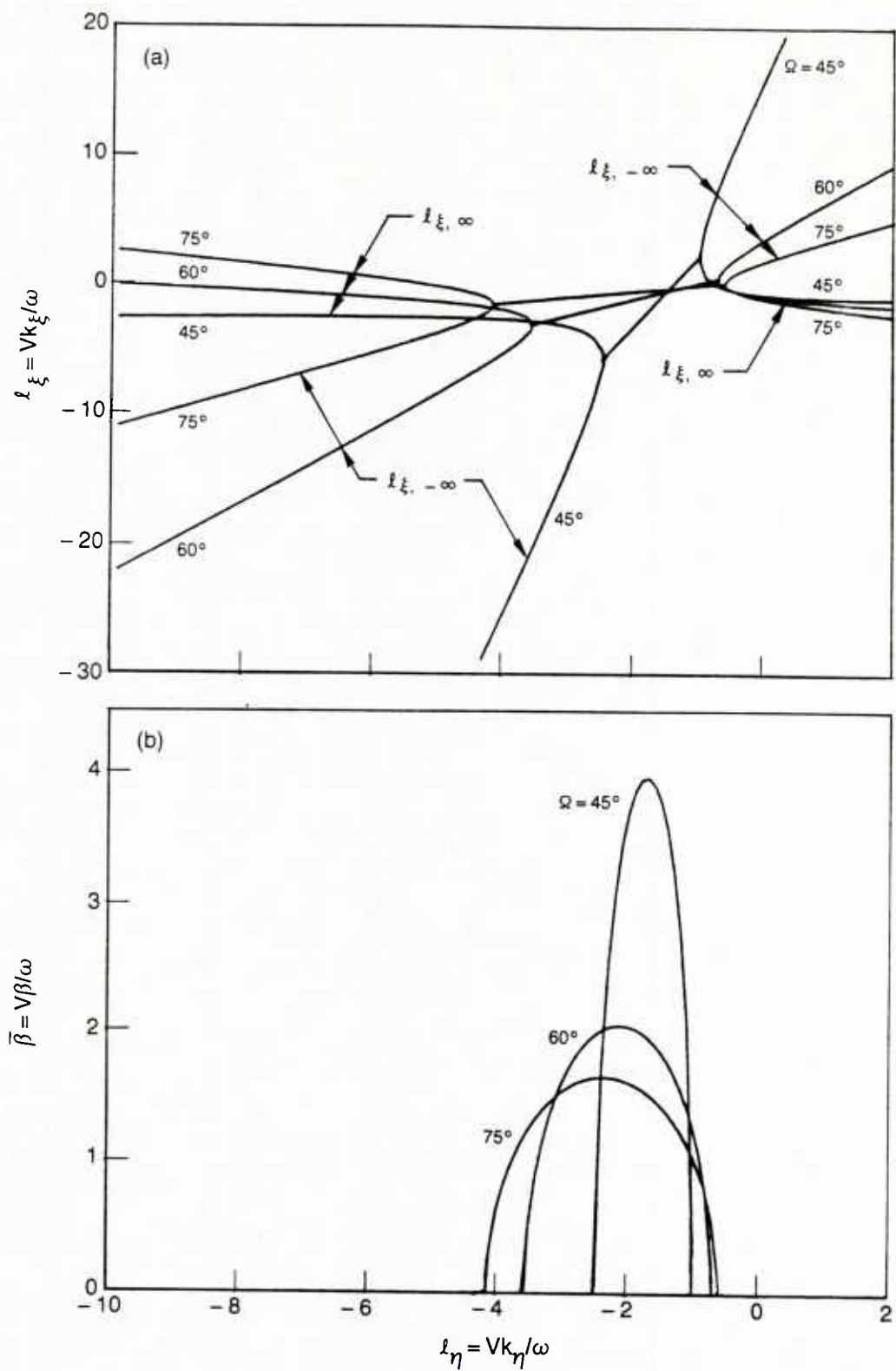
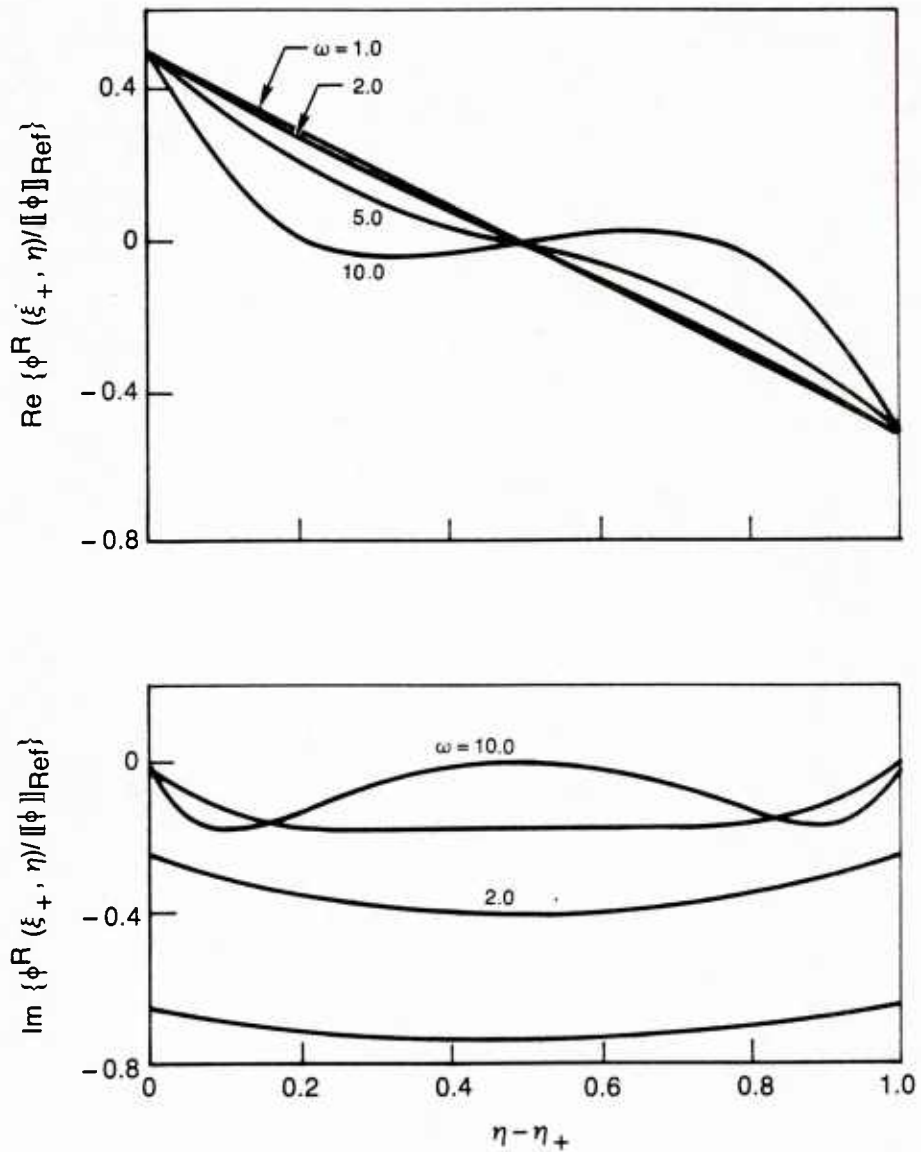


Figure 9. Effect of flow angle on the far-field acoustic response of an isolated blade row operating in a supersonic free stream; $M = 1.3$: (a) and (b) as in figure 8.



**Figure 10. The potential response to concentrated wake vorticity;
 $G = 1$, $V_\infty = 1$, $\Omega_\infty = 45$ deg, $\sigma = 0$.**

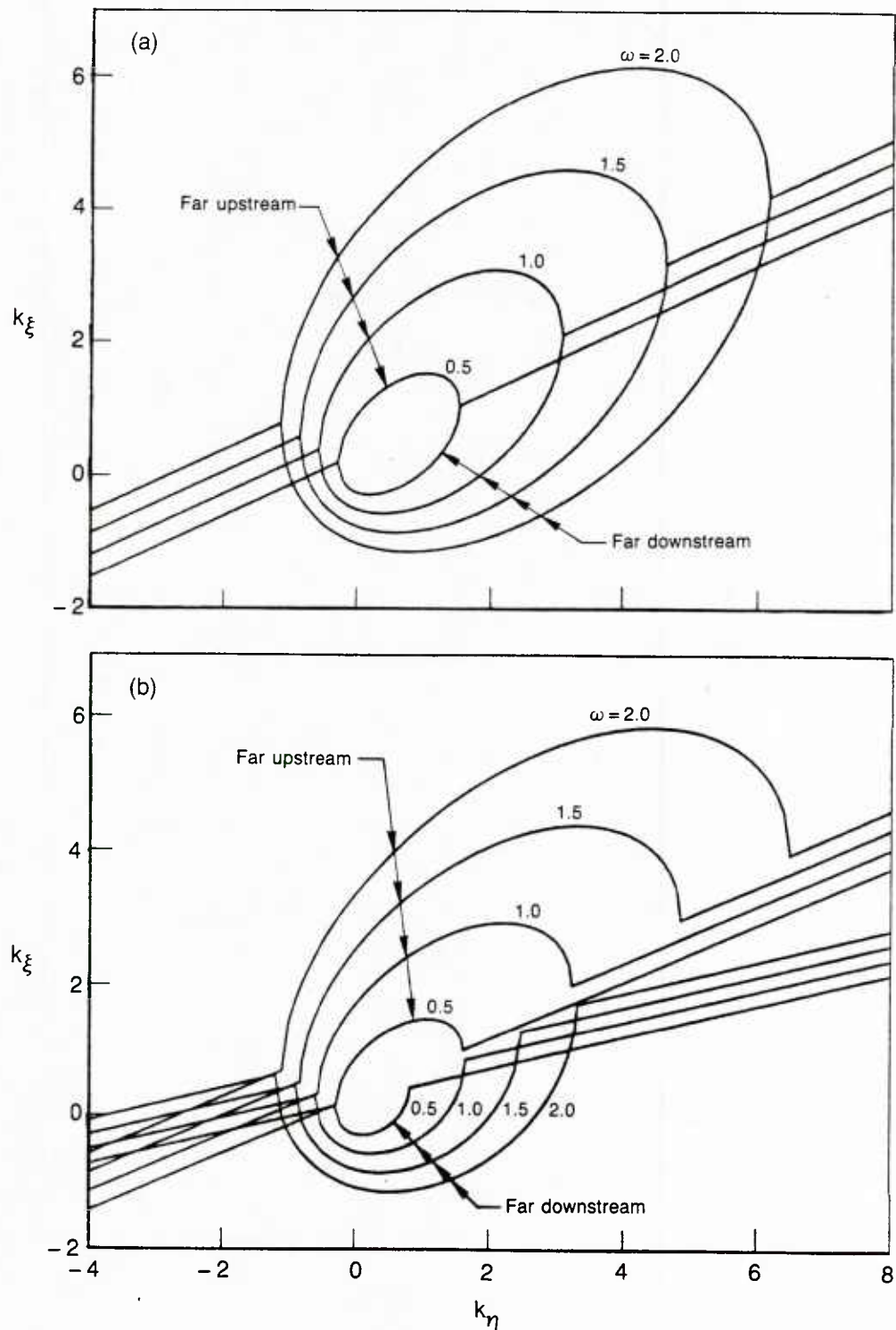


Figure 11. Axial vs. circumferential wave number of the far-field acoustic response associated with the example cascades; $G = 1$, $\Theta = 45$ deg: (a) flat-plate cascade; $M = 0.8$, $\Omega = 45$ deg; (b) DCA cascade; $M_\infty = 0.8$, $\Omega_\infty = 49.4$ deg, $M_\omega = 0.62$, $\Omega_\omega = 43$ deg.

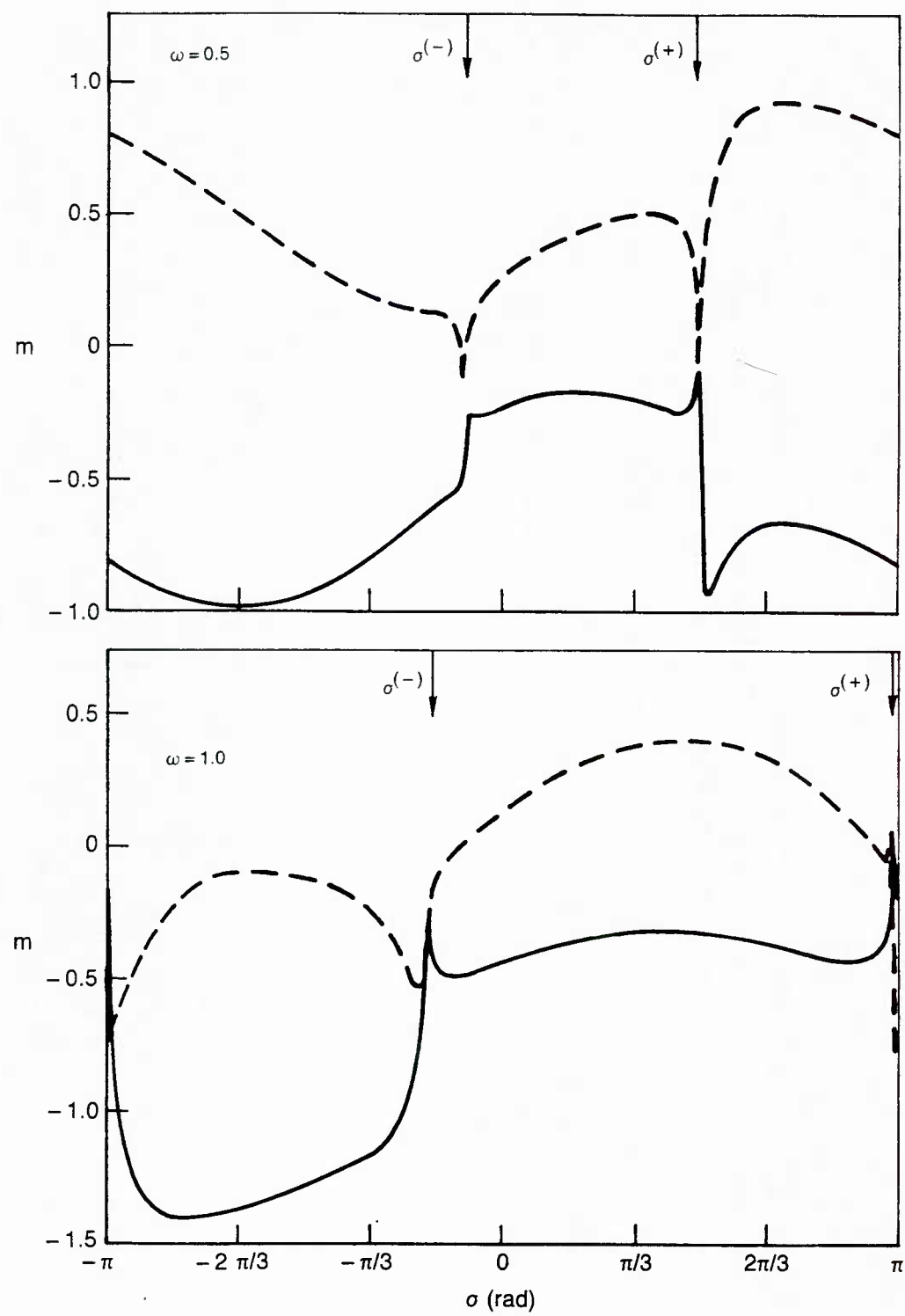


Figure 12. Unsteady moment vs interblade phase angle for torsional blade vibrations of the example flat-plate cascade: —— in-phase component (real part); —— out-of-phase component (imaginary part).

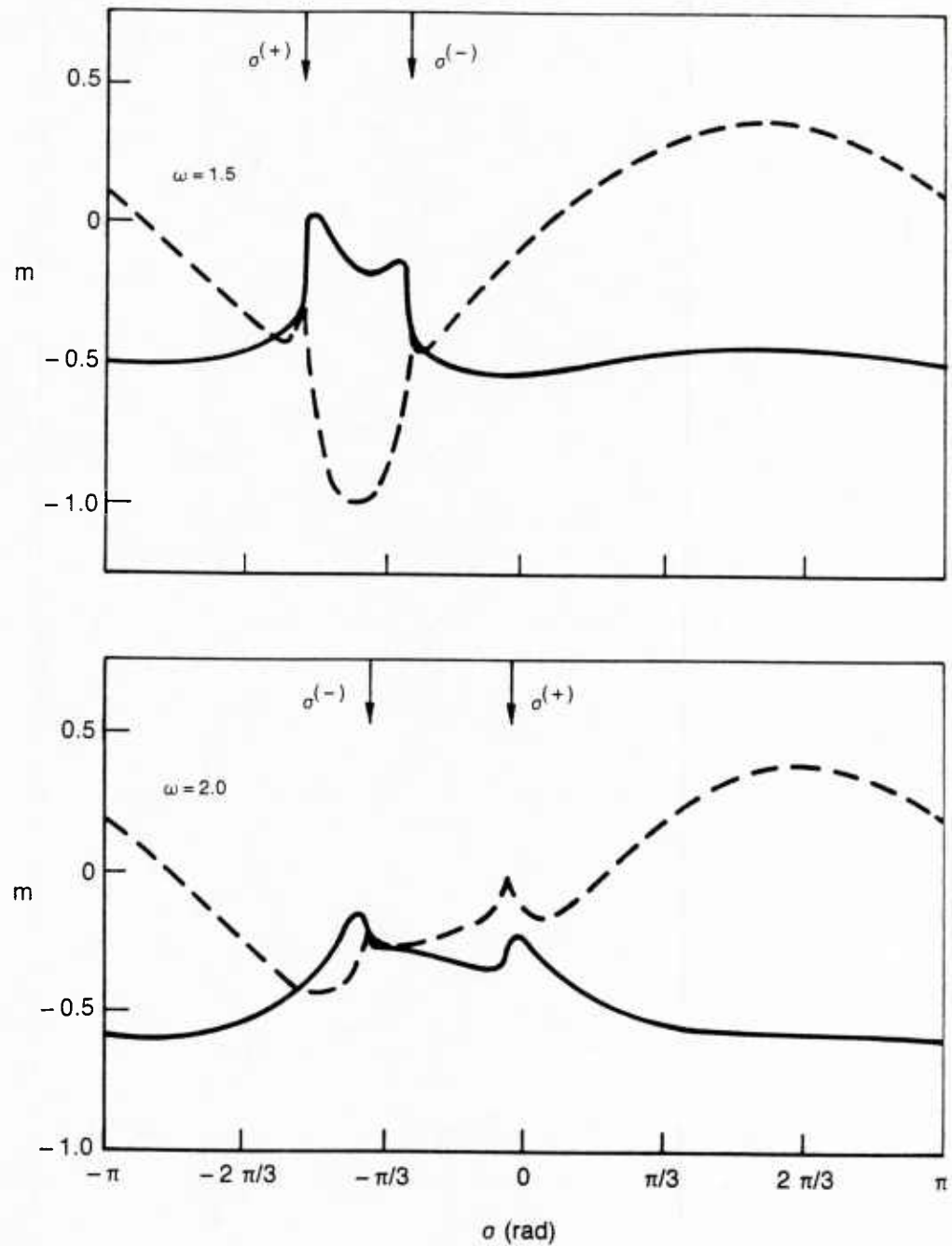


Figure 12. (cont.) Unsteady moment vs interblade phase angle for torsional blade vibrations of the example flat-plate cascade: — in-phase component (real part); — out-of-phase component (imaginary part).

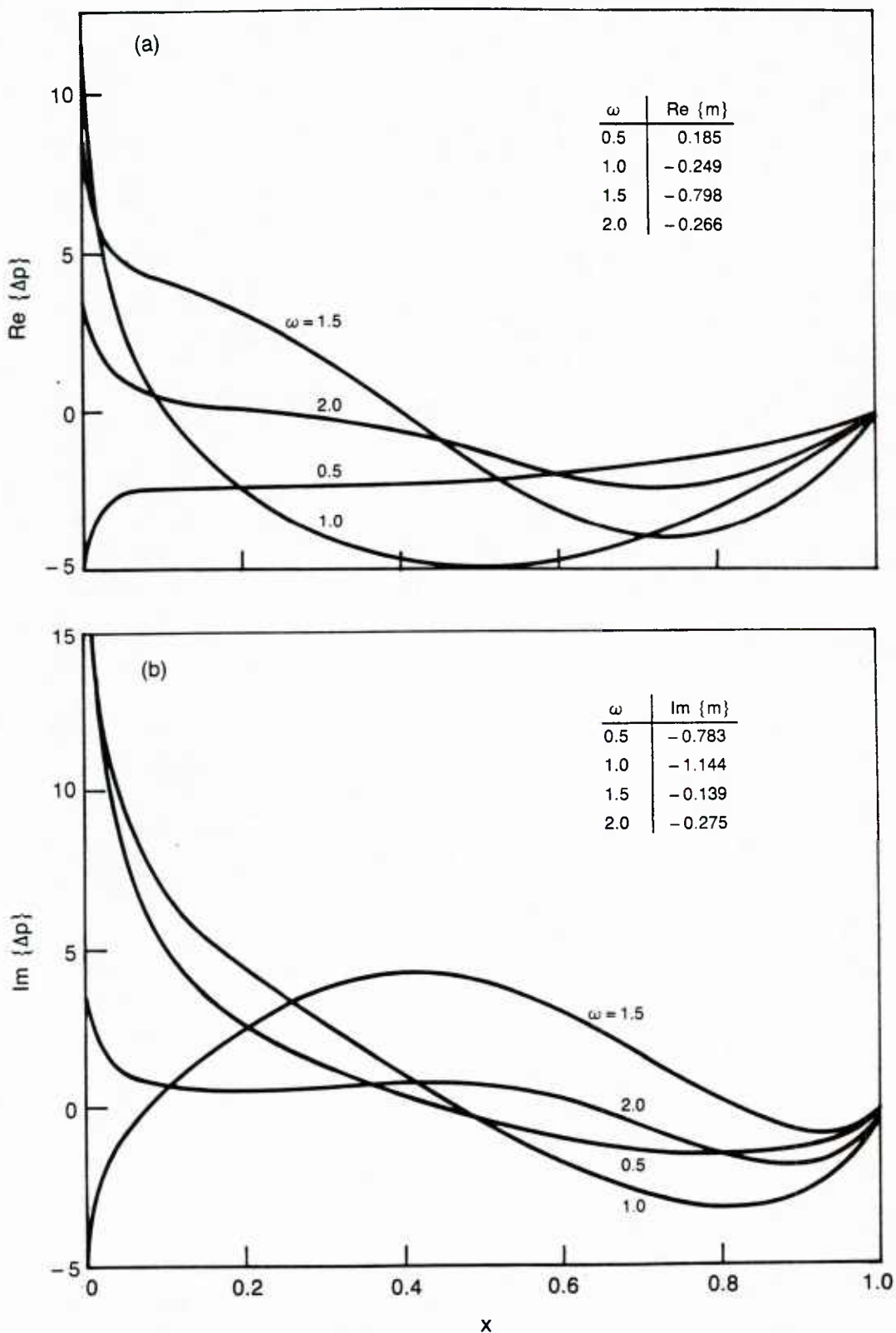


Figure 13. Unsteady pressure difference distributions due to torsional blade vibrations at $\sigma = -1$ for the example flat-plate cascade: (a) in-phase component; (b) out-of-phase component.

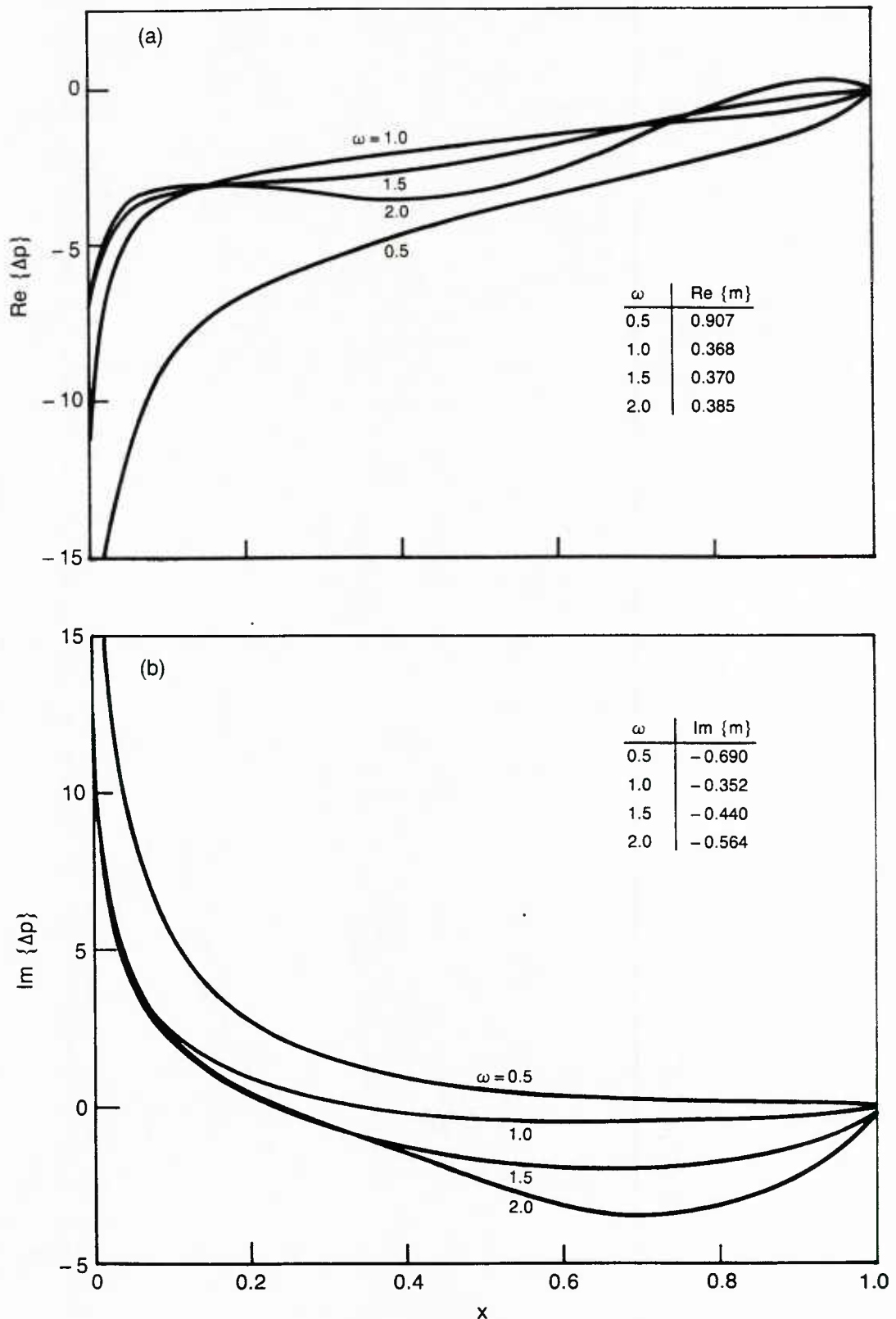


Figure 14. Unsteady pressure difference distributions due to torsional blade vibrations at $\sigma = 2$ for the example flat-plate cascade: (a) in-phase component; (b) out-of-phase component.

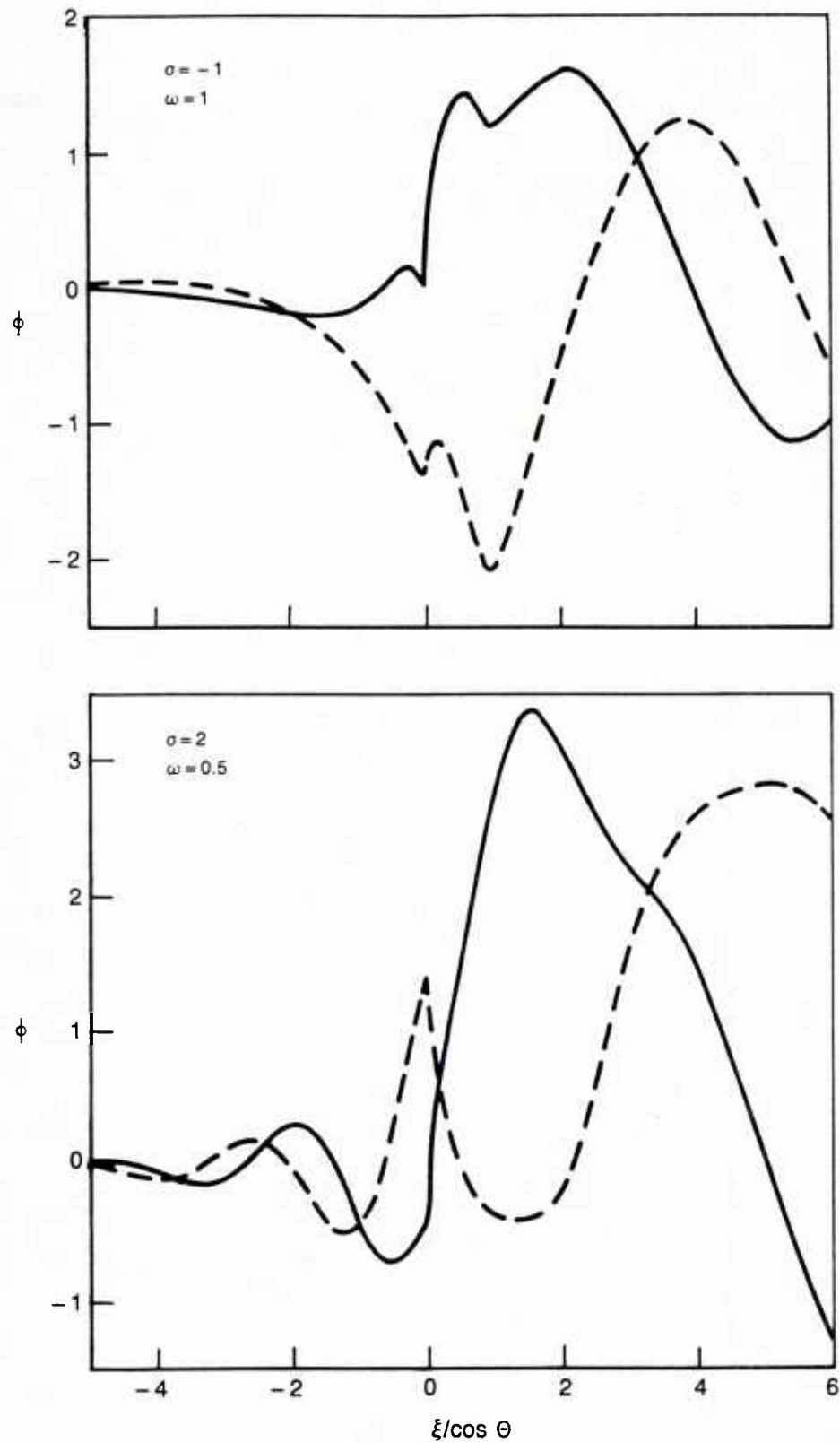


Figure 15. Unsteady potential distributions on $y=0^+$ for torsional blade vibrations of the example flat-plate cascade; numerical solution domain extends over $-1 \leq \xi/\cos \theta \leq 2$: — in-phase component; —— out-of-phase component.

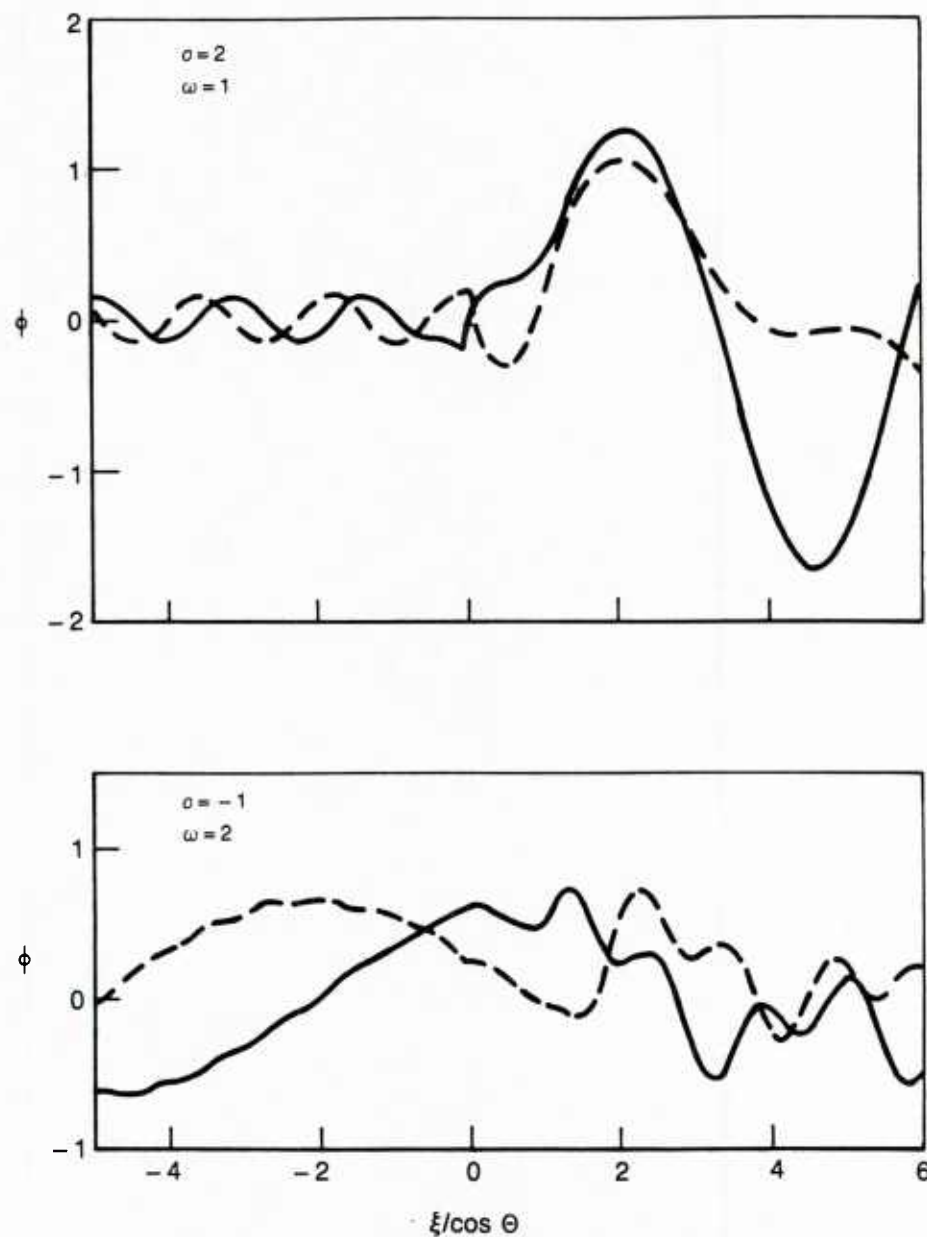


Figure 15. (cont.) Unsteady potential distributions on $y=0^+$ for torsional blade vibrations of the example flat-plate cascade; numerical solution domain extends over $-1 \leq \xi/\cos \Theta \leq 2$:
-- in-phase component; —— out-of-phase component.

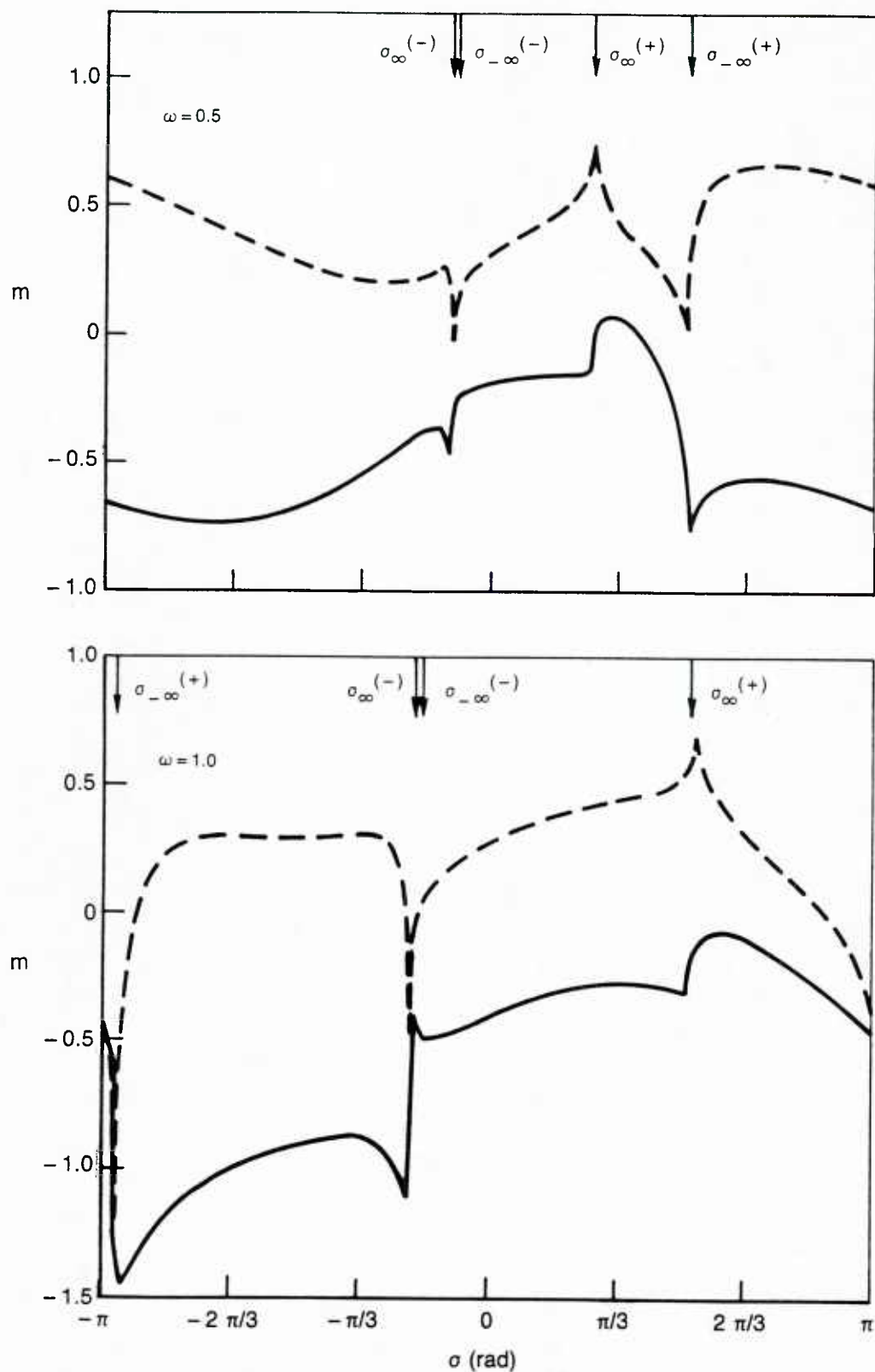


Figure 16. Unsteady moment vs interblade phase angle for torsional blade vibrations of the example DCA cascade: — in-phase component (real part); — out-of-phase component (imaginary part).

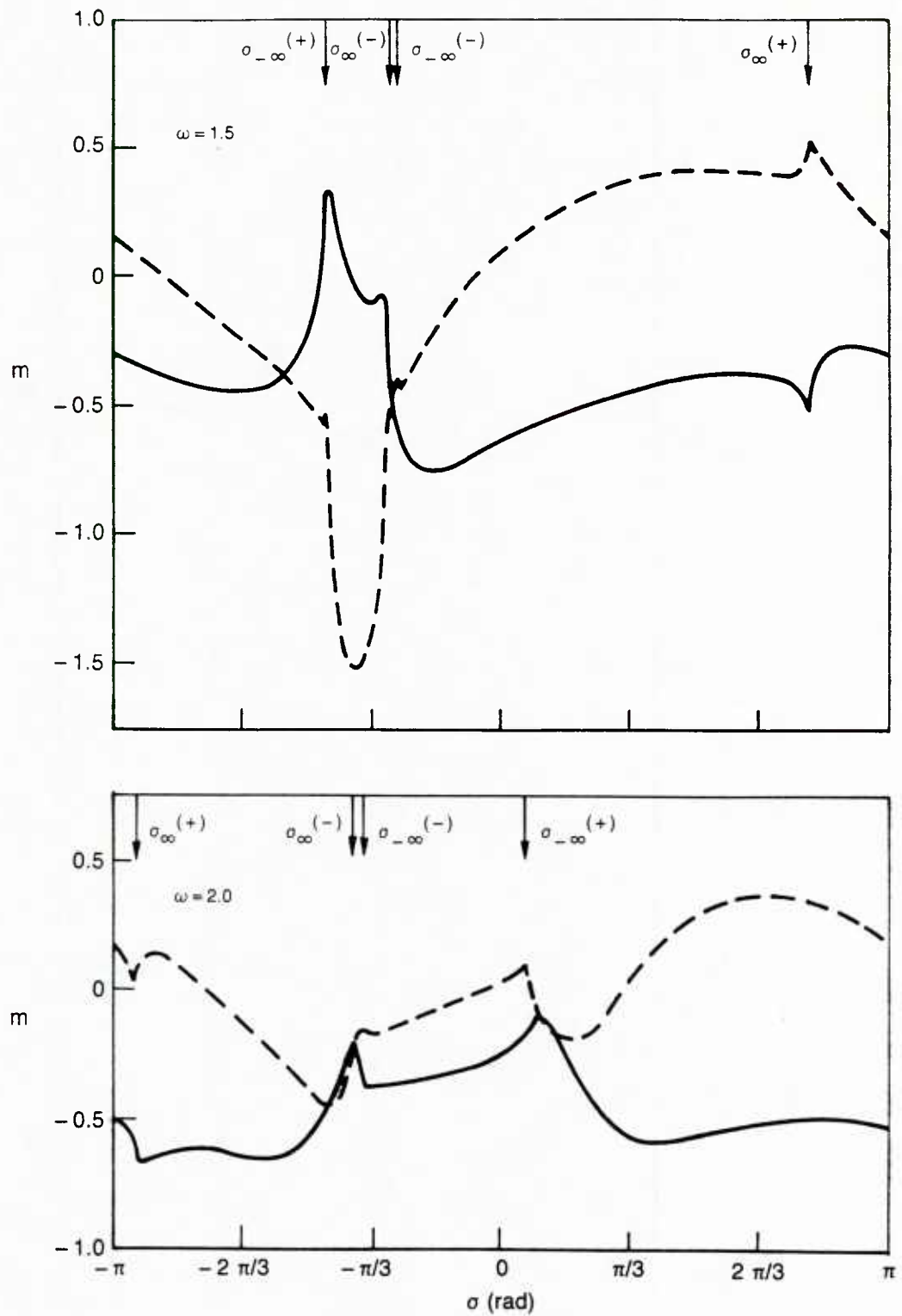


Figure 16. (cont.) Unsteady moment vs interblade phase angle for torsional blade vibrations of the example DCA cascade: —— in-phase component (real part); —— out-of-phase component (imaginary part).

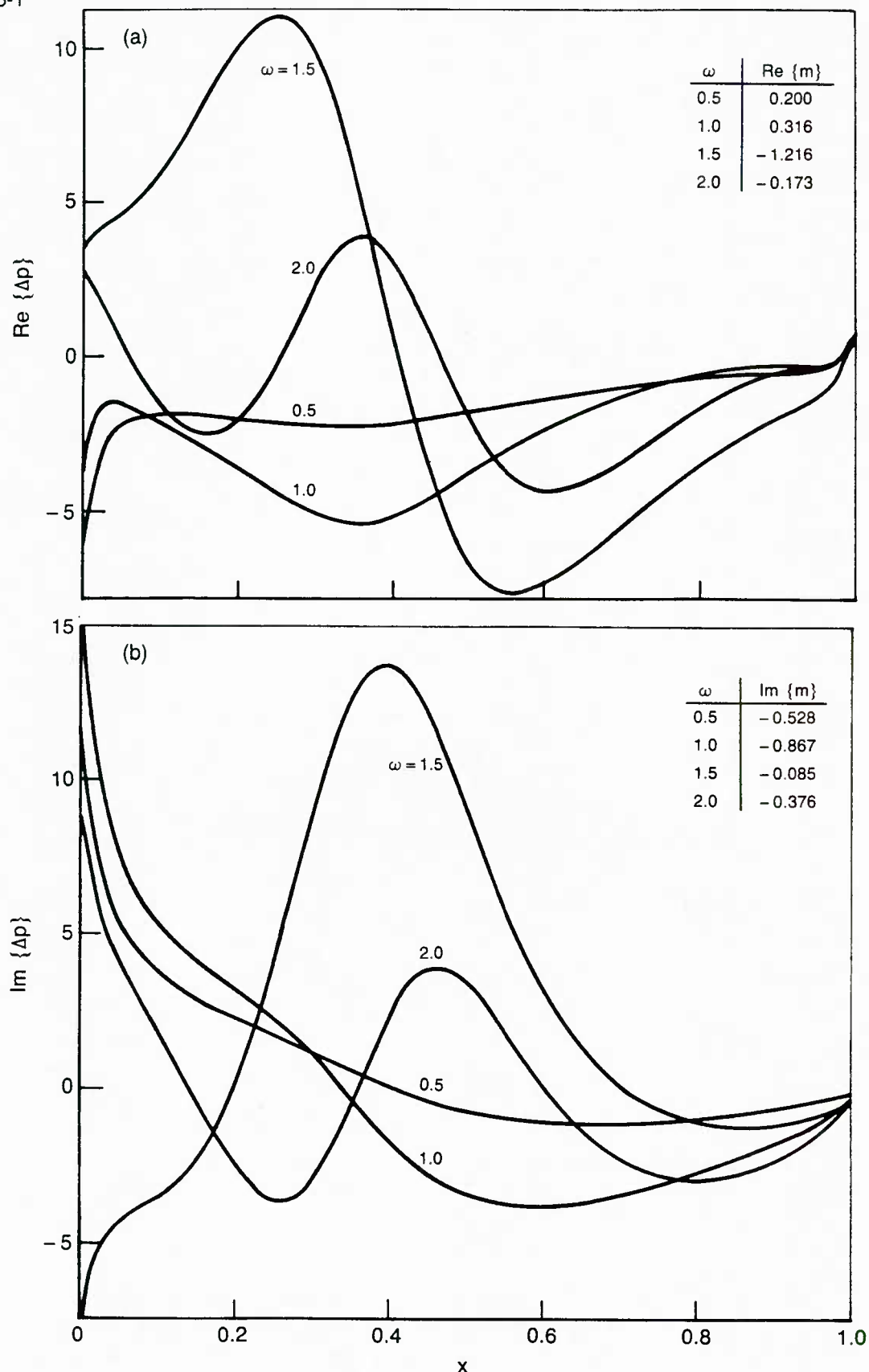


Figure 17. Unsteady pressure difference distributions due to torsional blade vibrations at $\sigma = -1$ for the example DCA cascade: (a) in-phase component; (b) out-of-phase component.

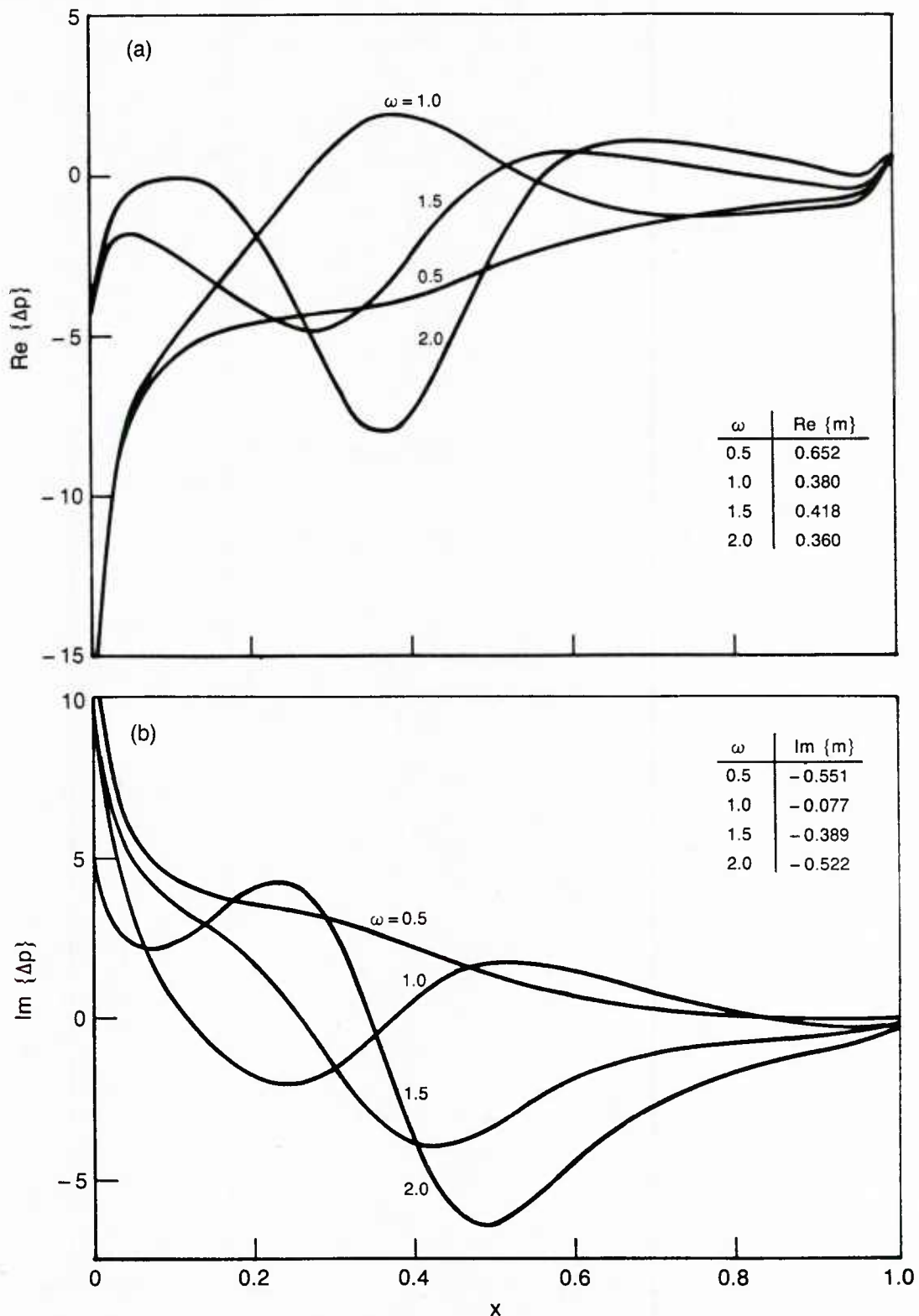


Figure 18. Unsteady pressure difference distributions due to torsional blade vibrations at $\sigma=2$ for the example DCA cascade: (a) in-phase component; (b) out-of-phase component.

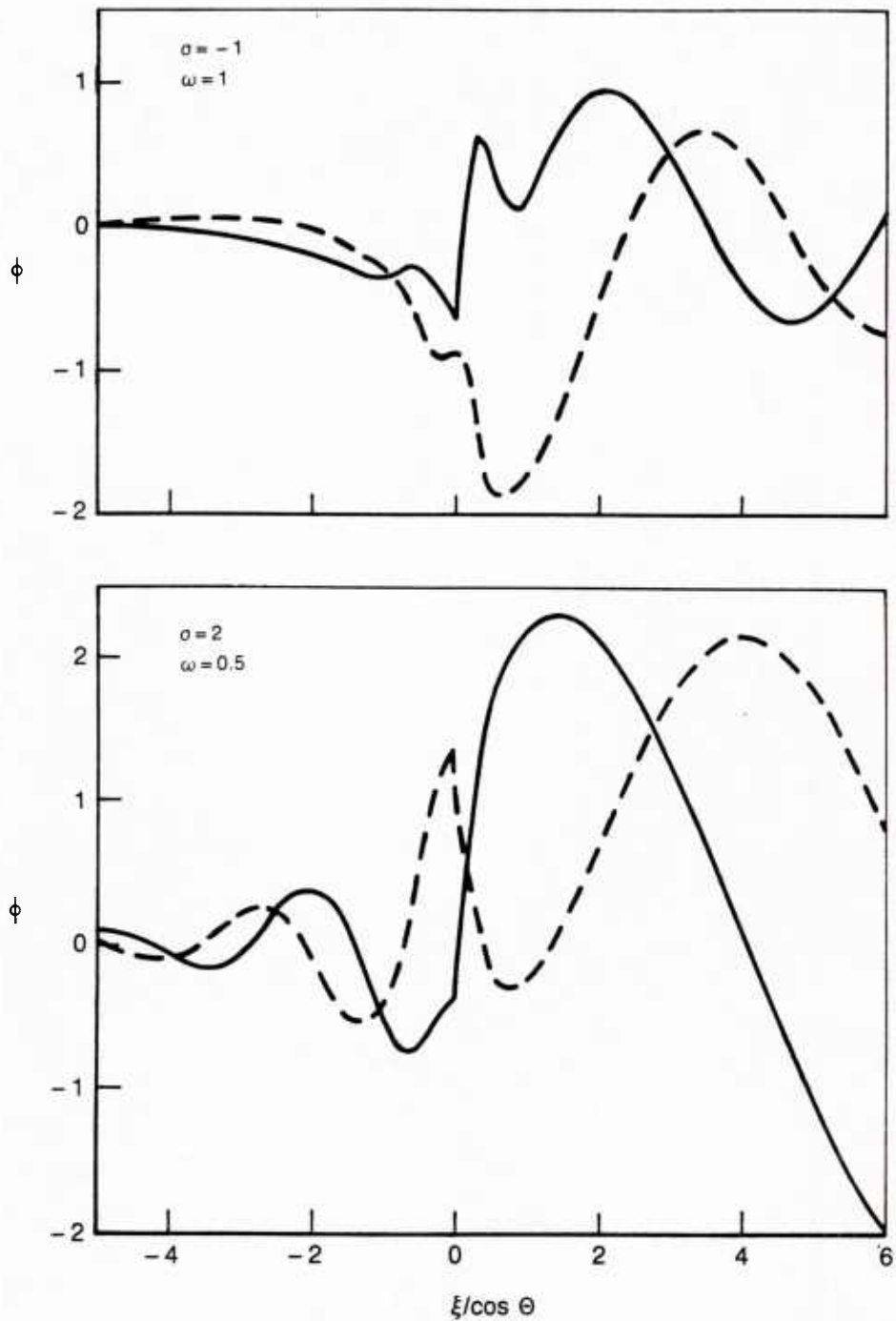


Figure 19. Unsteady potential distributions along the reference stagnation streamline for torsional blade vibrations of the example DCA cascade; numerical solution domain extends over $-1 \leq \xi/\cos \theta \leq 2$: — — in-phase component; — out-of-phase component.

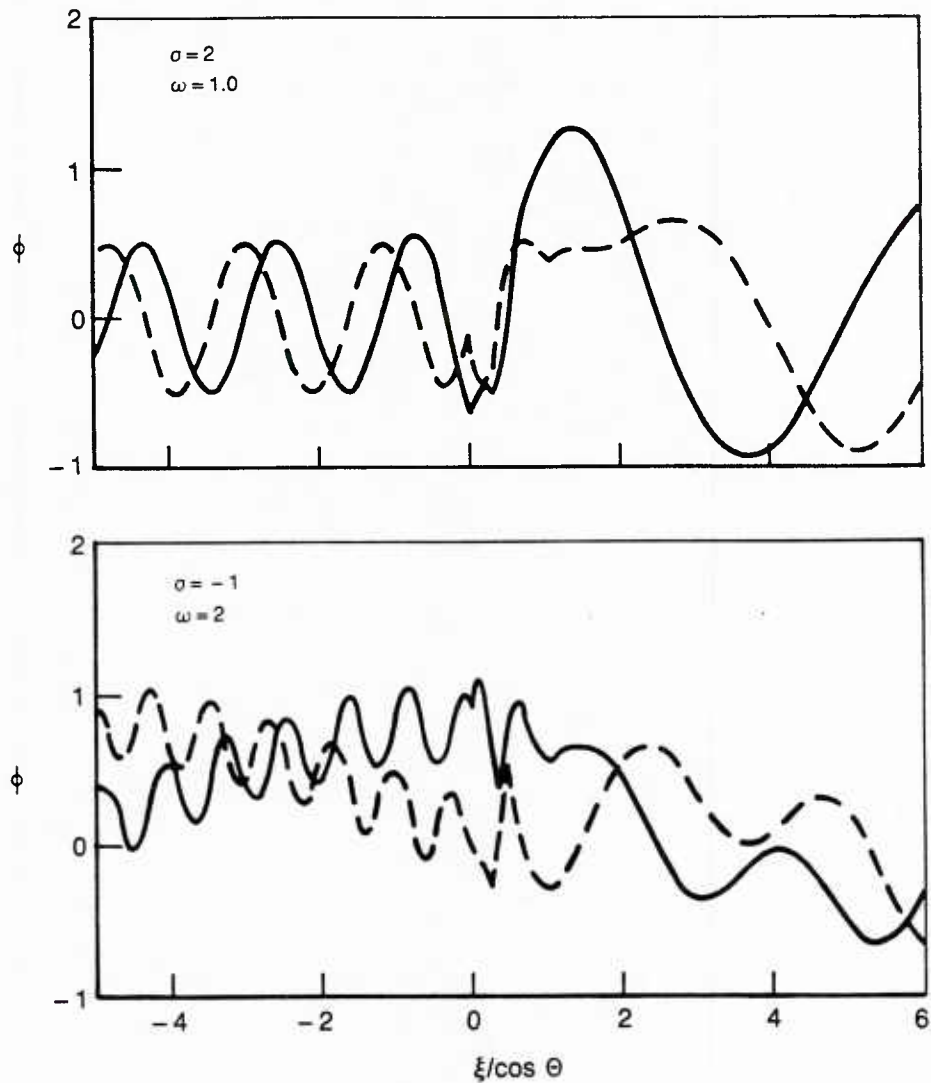


Figure 19. (cont.) Unsteady potential distributions along the reference stagnation streamline for torsional blade vibrations of the example DCA cascade; numerical solution domain extends over $-1 \leq \xi/\cos \theta \leq 2$: — in-phase component; — out-of-phase component.

U230940